The Status of the Tropical Rainfall Measuring Mission (TRMM) after 2 Years in Orbit

C. Kummerow, J. Simpson, O. Thiele, W. Barnes, A.T.C. Chang, E. Stocker, R. F. Adler, A. Hou

NASA/Goddard Space Flight Center, Greenbelt, Maryland

R. Kakar

NASA Headquarters, Washington DC

F. Wentz, P. Ashcroft

Remote Sensing Systems, Santa Rosa, California

T. Kozu

Shimane University, Shimane, Japan

Y. Hong

Caelum Research Corporation, Rockville, Maryland

K. Okamoto, T. Iguchi, H. Kuroiwa

Communications Research Laboratory, Tokyo, Japan

E. Im, Z. Haddad

Jet Propulsion laboratory, Pasadena California

G. Huffman

Science Systems and Applications, Inc., Lanham, Maryland

T. Krishnamurti

Florida State University, Tallahassee, Florida

B. Ferrier, W.S. Olson

University of Maryland, Baltimore County

E. Zipser

University of Utah, Salt lake City, Utah

E.A. Smith

NASA/Marshall Space Flight Center

T.T. Wilheit, G. North

Texas A&M University, College Station, TX

K. Nakamura

Nagoya University, Nagoya, Japan

Abstract

The Tropical Rainfall Measuring Mission (TRMM) satellite was launched on November 27, 1997, and data from all the instruments first became available approximately 30 days after launch. Since then, much progress has been made in the calibration of the sensors, the improvement of the rainfall algorithms, in related modeling applications and in new datasets tailored specifically for these applications. This paper reports the latest results regarding the calibration of the TRMM Microwave Imager, (TMI), Precipitation Radar (PR) and Visible and Infrared Sensor (VIRS). For the TMI, a new product is in place that corrects for a still unknown source of radiation leaking in to the TMI receiver. The PR calibration has been adjusted upward slightly (by 0.6 dBZ) to better match ground reference targets, while the VIRS calibration remains largely unchanged. In addition to the instrument calibration, great strides have been made with the rainfall algorithms as well, with the new rainfall products agreeing with each other to within less than 20% over monthly zonally averaged statistics. The TRMM Science Data and Information System (TSDIS) has responded equally well by making a number of new products, including real-time and fine resolution gridded rainfall fields available to the modeling community. The TRMM Ground Validation (GV) program is also responding with improved radar calibration techniques and rainfall algorithms to provide more accurate GV products which will be further enhanced with the new multiparameter 10-cm radar being developed for TRMM validation and precipitation studies. Progress in these various areas has, in turn, led to exciting new developments in the modeling area where Data Assimilation, and Weather Forecast models are showing dramatic improvements after the assimilation of observed rainfall fields.

1. Motivation and history of TRMM

Tropical rainfall is important in the hydrological cycle and to the lives and welfare of humans. Three-fourths of the energy that drives the atmospheric wind circulation comes from the latent heat released by tropical precipitation. Precipitation, unfortunately, is one of the most difficult atmospheric parameters to measure because of the large variations in space and time. Tropical rainfall oscillates wildly between severe droughts and occasional deadly floods. Yet, it often lasts no longer than a few hours at a time. Until the end of 1997, precipitation in the global tropics was still very uncertain with large numbers of infrared and passive microwave algorithms providing very diverse estimates. Regarding "global warming", the various large-scale models differed among themselves in the predicted magnitude of the warming, distribution and amount of tropical precipitation, and in the expected regional effects of these temperature and moisture changes. Accurate estimates of tropical precipitation were desperately needed in order to validate and gain confidence in these models.

The idea of measuring rainfall from space using a combined instrument complement of passive and active microwave (radar) instruments was generated in the early 1980's. By September 1984, a proposal entitled "Tropical Rain Measuring Mission" was submitted to Dr. Theon at NASA Headquarters by a team of Goddard investigators consisting of Drs. North, Wilheit and Thiele. Japan's Communications Laboratory, then headed by Dr. Fugono, joined in the activities soon thereafter. Joint aircraft flights with an experimental radar (Meneghini *et al.*, 1992) suggested that instrument accuracy was promising. The low Earth orbit needed to realize such measurements from a spaceborne platform, however, immediately raised concerns regarding the sampling adequacy of such a satellite.

The radar data from the four GATE ships stationed in the Intertropical Convergence Zone (ITCZ) off Africa in 1974 were used for a series of sampling studies. Several orbits and altitudes were considered. An inclined orbit extending between 35°N and 35°S at 350 km altitude was found to be most suitable. The inclined orbit precessed such that the satellite would overfly a given location at a different time every day with a 30 day cycle. This would allow the documentation of the large diurnal variation of tropical rainfall. The altitude of 350 km was satisfactory from the radar antenna requirements. Shin and North (1988, in draft form by the summer of 1986) showed that in the wet tropical areas the sampling errors for monthly accumulations in 5°x5° grids would be less than 10%. Shin and North also showed that with rain data from another satellite, such as the SSM/I passive microwave radiometers onboard military satellites, the sampling errors could be cut in half and useful data could be obtained in drier environments as well.

Insuring the credibility of space-based measurements of rainfall was also a concern from the onset because of the considerable difficulty of making accurate rain measurements via conventional means. Thus, the need for reliable surface-based observations for validating TRMM satellite measurements was established. The ground validation program that followed included studies to improve rainfall measurement technology; establishment of ground validation sites consisting of radars, rain gauges and disdrometers around the tropics; developing and expanding techniques to measure rainfall in oceanic regions; improving ground based rainfall estimation techniques; and developing radar processing and analysis software for producing and analyzing Ground Validation (GV) products. To complement the surface-based measurements, the planning for extensive field campaigns was initiated early to provide the necessary microphysical and dynamical structure of convective systems in the tropics after launch.

In November of 1985, the first major workshop was convened near Goddard to further develop the proposed "Tropical Rainfall Measuring Mission". Many participants from this meeting soon organized into a more formal Science Steering Panel headed by Dr. Rasmusson. This group released a report establishing the science priorities for mission in 1986. These goals are given in Table 1.

Although tropical precipitation is organized on the mesoscale, it is noteworthy that the primary objectives of the mission were to improve climate models and aid them in climate prediction. It was proposed to have a dual frequency radar, a multi-channel dual polarized, conically scanning passive microwave instrument similar to SSM/I, a single frequency cross-track scanning radiometer to sample along with the radars, and a Visible/Infrared radiometer similar to the AVHRR. The purpose of the Visible/Infrared instrument was to enable TRMM to be a "flying rain gauge". The dual frequency radar and radiometer combination would be able to derive high quality precipitation profiles. The small cloud drops that play an integral part in the latent heat release process, however, would not be observable with sufficient accuracy to construct vertical profiles. It was therefore planned from the start to use results of a cloud-resolving numerical model in retrieving the important latent heat profiles.

The encouraging results from the sampling and aircraft studies led NASA Headquarters to select TRMM from a number of competing proposals from atmospheric scientists proposing low-cost atmosphere missions. In 1986, the Japanese Space Commission accepted an invitation to jointly study the feasibility of TRMM. In 1987, NASA designated TRMM as an Earth Probe, but decided in the spring of 1988, that the Phase A budget estimate for TRMM exceeded Earth Probe specifications. The Science Steering Group therefore decided to descope the radar to a single frequency at 14 GHz. The cross-track scanning radiometer was also eliminated. In addition, the resolution of the Infrared sensor was reduced from 1 to 2 km, and the number of data products planned for the Data System was reduced to the

minimum needed for rainfall purposes. Agreements between the US and Japan were formalized in 1988, leading to a New Start for a joint US/Japan mission at that time. The Japanese agreed to provide the precipitation radar and a launch by their new HII Rocket. NASA would provide the spacecraft and the other rain sensing instruments.

TRMM advanced to Phase B (final design) in the fall of 1989. The modified version of the Science Steering Group report was published before the end of the year (Simpson, Ed., 1988). TRMM received strong endorsement in the United States by National Research Council and the Joint Federal Agency's reviews. Then, in January 1990, the U.S. budget for Earth Probes was eliminated for 1991. To overcome this setback, key members of the U.S. and Japanese science communities expressed their urgent need for the tropical rainfall data to several high-placed authorities. As a consequence of their efforts, the U. S. Congress passed support for TRMM for a New Start in 1991, and the project got formally underway.

At this time, two important decisions were made. The first was to slightly enhance the now single passive microwave radiometer to include a channel at 10 GHz. This was important to avoid saturation from the heavy tropical rainfall. The second was to accommodate two EOS instruments, namely a Lightning Imaging Sensor (LIS) and a Cloud and Earth Radiant Energy System (CERES) to measure the total upwelling radiant energy.

In early 1991, the first TRMM U.S. three-year Science Team was selected from about 100 proposals (23 members from U.S., 8 foreign members). Many meetings and Workshops on algorithms and validation took place in both U.S. and Japan, with results to be discussed in the next Section. In 1993, the TRMM Observatory passed its Critical Design Review and moved into Phase C/D of actual Observatory construction. In 1994, the U.S. and Japan simultaneously selected new science teams that would be in place until the launch of TRMM in 1997. While it was decided that the two teams should operate independently, a Joint

TRMM Science Team made up of Team Leaders from both countries was established to coordinate the efforts of both teams. This joint team has worked effectively since then through the successful launch of TRMM from Tanegashima island on the morning of Nov. 28, 1997 (afternoon of Nov. 27 in the US) to the present time.

2. TRMM Instruments and Instrument Data

2.1 The final instrument complement

The final TRMM instrument complement is shown in Table 2. While neither the second radar frequency nor the cross-track scanning radiometer were included, the extra 10 GHz channel was included on the multi-frequency radiometer, greatly strengthening the passive microwave products.

TRMM's Precipitation Radar (PR) is the first radar designed specifically for rainfall monitoring to operate from space. While its swath is relatively narrow and it suffers from the same uncertainties for rainfall estimation as ground based radars, the TRMM PR has delivered an incredible wealth of detailed rain structure information. Examples include the studies of propagating rainfall structures across land and ocean by Takayabu *et al.*, (1999), the direct observational evidence for the suppression of rainfall by smoke contaminated clouds done by Rosenfeld (1999), the improvement of passive microwave rainfall retrievals, and methods for potentially using PR as a reference standard to cross calibrate ground based radars. The passive microwave instrument, TMI, aside from providing the highest resolution data available to date, also has been used to derive sea surface temperature by a number of investigators (e.g. Wentz, 1999). The combination passive and active sensors has, in turn, allowed researchers to look into further constraining parameters such as the Drop-Size-Distribution (DSD), Haddad *et al.*, (1997) or Viltard *et al.*, (1999). The Visible and infrared instrument, in turn, has been useful to relate the detailed TRMM observations to the more

available data from geostationary satellite data. It also has played in a key role in interpreting early results from the CERES instrument.

The instrument characteristics themselves are not treated here as they are described in detail in the available literature. The core TRMM instrument, PR, TMI and VIRS are described in (Kummerow *et al.*, 1998). The LIS instrument is described in (Christian *et al.*, 1992), and the CERES instrument is described by (Lee *et al.*, 1998).

Calibrated and Earth located data from the TRMM instruments is referred to as Level 1 data. Coding of the Level 1 algorithms was performed by the TRMM Science and Data Information System (TSDIS) for the TMI and VIRS, and by NASDA for the PR. The only additional product at level 1 is the PR reflectivity. In this algorithm the radar returned power is converted into reflectivity, the factors most often used in science applications. In addition to the conversion, a decision is made regarding the existence of rain in the radar filed of view. If no rain is detected, the entire reflectivity column is set to a missing value. This was done to help reduce data volumes in compressed file formats. All TRMM products have version numbers that are incremented each time the data are reprocessed to reflect an advancement of the TRMM products. Beginning with Version 3 at launch (Version 1 & 2 were pre-launch test codes), the data have been reprocessed to version 4 beginning on Sept. 1, 1998, and Version 5 beginning on Oct. 1, 1999.

2.2 Instrument Calibration

2.2.1 TMI Calibration

Almost immediately after launch, a calibration problem was detected with the TMI instrument. To obtain a consistent time series of geophysical parameters from SSM/I and TMI, the TMI was intercompared with the SSM/I's. The SSM/I's on F11, F13, and F14 are used for the inter-calibration. TMI Level 1B data and SSM/I daily 1.0° maps from 12/10/97

through 4/24/98 were spatially collocated to within 0.7° and temporally collocated to within 30 minutes. To best compare TMI and SSM/I antenna temperatures (T_A), two corrections for instrumental differences were applied. The TMI incidence angle is slightly different (52.75° versus 53.4° for SSM/I) and the TMI water vapor channel is at 21.3 GHz rather than 22.235 GHz. Thus, the SSM/I T_A's must be adjusted to correspond to the TMI incidence angle and frequencies before comparisons can be made. Over the ocean, the magnitude of the incidence angle adjustment is about 1K, while the frequency adjustment can be as large as 10 K. These adjustments are not constant, but depend on the atmospheric transmittance. No adjustment is made to land observations because (1) the incidence angle and frequency dependence of T_A is small and (2) there are no reliable models for the incidence angle and frequency variation of land observations.

Using collocated T_A, the joint probability density function of $T_{A,TMI}$ - $T_{A,SSM/I}$ and $T_{A,SSM/I}$ was formed for each channel. Results are shown in Figure 1 represent the weighted least-squares fit to the data. The fit can be expressed in terms of the following equation:

$$T_{A,SSMI} = a_1 T_{A,TMI} + a_0 \tag{1}$$

For all channels, the difference between SSM/I and TMI is near zero near T_A = 295 K and increases linearly with decreasing T_A. For cold ocean observations the bias reaches values as high as 5 K. The TRMM rollover maneuver also indicates that $T_{A,TMI}$ has a warm bias. For comparison, the inter-calibration biases for the series of SSM/I platforms were typically only about 0.5 K. Thus the series of SSM/I's showed much better agreement than does TMI.

After some analysis, it was decided to use the following error model:

$$T_{A,TMI} = (1-\varepsilon)T_A + \varepsilon T_0 \tag{2}$$

where T_A is the true temperature of the incoming radiation, $T_{A,TMI}$ is the measurement, T_0 is the physical temperature of some unknown emitter in the field of view (possibly the antenna itself), and ε is the emissivity of that emitter. Taking the SSM/I observations as truth (with

all the appropriate caveats), then (1) and (2) can be combined to obtain the following relationships:

$$\varepsilon = \frac{a_1 - 1}{a_1} \tag{3}$$

$$T_0 = \frac{-a_0}{a_1 - 1} \tag{4}$$

Thus one can use the SSM/I versus TMI comparison to estimate the temperature and emissivity of the error source. Table 3 gives the results. As can be seen, except at 85 GHz, which we have the least confidence in, the emitter temperature is similar to 295K and the emissivity is about 3 to 4 %. Since there are no SSM/I versus TMI comparisons at 11 GHz, we use the 19 GHz value to specify ε and T_0 at 11 GHz.

Given ε and T_0, (2) can then be used to predict $T_{A,TMI}$ for the TRMM rollover maneuver for which $T_A = 2.7$. The predicted difference between $T_{A,TMI}$ minus 2.7 is given in Table 2 under the column $\Delta T_{A,pred}$, and the T_A difference that was actually observed is given in the last column. There is generally good agreement between the cold space bias predicted from the SSM/I versus TMI comparison and that actually observed, thereby giving us confidence in the error model.

Two corrections are therefore possible to account for the emitting source that appears to be radiating into the TMI feedhorns. The first correction is simply the inverse of equation (2), where ε and T_0 come from Table 4.

$$T_A = \frac{T_{A,TMI} - \varepsilon T_0}{1 - \varepsilon} \tag{5}$$

Depending on the application, this correction has the additional advantage that it matches the TMI observations to the SSM/I observations so that one can produce a continuous time series.

The second correction is based on the TRMM rollover maneuver observations and the assumption that the error model given by (2) is correct and that the typical value for T_0 is 295 K. With these assumptions one has (note 292.3 = 295-2.7)

$$T_A = \frac{292.3T_{A,TMI} - 295\Delta T_{A,obs}}{292.3 - \Delta T_{A,obs}} \tag{6}$$

Beginning with Version 5, the TMI radiance data uses the rollover calibration procedure (eq'n 6). This was done in order to retain as much physics as possible and avoid potential errors that can be introduced by simply cross-calibrating sensors. Prior data (Versions 3 & 4) contain the warm bias error described above.

2.2.2 PR calibration

Accurate calibration of the PR is important to establish the clear interface condition between Level-1 and higher level algorithms, thereby assuring accurate and stable rain products. To develop the PR calibration algorithm, variation and drift of PR system parameters are modeled to have "intermediate-term", and "long-term" components. The former is caused by the temperature change inside the PR and roughly has a period of one orbit (91 min). The correction for this term can be performed by monitoring the temperature of the instrument. The long term variations may occur due to gradual degradation of system performance (gain, loss, etc.) and/or failure of some active array elements. To monitor this term, an internal loop-back calibration function, including transmitter power and receiver gain monitors have been implemented. To conduct an absolute calibration and to detect changes in antenna characteristics and telemetry sensors, a calibration scheme using an external reference target has also been developed.

An internal calibration algorithm has been developed using a detailed PR system model that describes the temperature dependence of all system parameters related to the conversion process from count value to the radar received power or to the radar reflectivity factor. The internal calibration handles the relative intermediate-term variation and some part of the long-term variation through the measurement of the input-output characteristics of the

receiver. External calibration of the PR, which handles the absolute calibration and monitoring of long-term variations, is performed using an Active Radar Calibrator (ARC) placed at a ground calibration site in Japan. An error budget analysis of the ARC calibration, including the error in the internal calibration, has indicated that the absolute calibration accuracy of better than 1 dB could be achieved.

In the initial check-out of the PR, which was conducted for 2 months after the TRMM launch, the PR system gain was determined through ARC calibrations. As a result, it was confirmed that the calculated PR receiver gain, based on the data obtained on the ground before launch, and using the temperature telemetry, is about 0.6 dB higher than the ARC calibration result, while the PR transmit power is about 0.6 dB lower. Those results were implemented as correction factors to calculate the PR received power and radar reflectivities. They are first implemented in Version 5 of the PR Level 1 products. Since the completion of the initial check-out, the PR system characteristics have shown excellent stability except for cases where unusual temperature change occurred due to power shutdown for satellite maintenance. Both transmit and receive path gains calibrated by the ARC have shown variations within +/- 0.2 dB around the gain initially corrected. Sea surface return levels measured at the incidence angles between 6 and 10 degrees are quite consistent with previous measurements by Ku-band airborne radars developed by Jet Propulsion Laboratory and Communications Research Laboratory, and have also been stable within about +/- 0.2 dB. Moreover, comparisons of PR-measured radar reflectivities of rainfall with those measured at NASA's Florida ground validation site and by the MU radar of Kyoto University show good agreements (differences within about 1 dB, on average). Those calibration and validation results indicate that the PR system characteristics have been and will be sufficiently stable and accurate to assure quantitative radar reflectivity and surface radar cross-section measurements.

Such agreement in the observed radar reflectivity has, in turn, forced a much more comprehensive validation strategy in order to assess the validity of rainfall products. It has also led to unforeseen benefits such as the possibility of using a spaceborne radar as a calibration constant to monitor the multitude of ground based radars which are calibrated independently and rarely to the 1 dBZ standards of the TRMM PR. An example of PR data collected over hurricane Floyd is shown in Figure 2.

2.2.3 VIRS Calibration

The VIRS radiometric calibration algorithm converts the digital data downlinked from the instrument into spectral radiances. VIRS has five bands, one in the visible, one in the shortwave infrared, and three in the thermal infrared. The calibration algorithm treats each band in the same manner, except that the visible and shortwave infrared bands do not respond to the thermal radiation emitted by the instrument and these bands do not have the nonlinear responses with input radiance found in the thermal bands. The calibration coefficients for the visible and shortwave infrared bands were determined in the laboratory before launch. VIRS carries a reference blackbody that is used to update the calibration coefficients for the thermal bands for each scan of the instrument on orbit. In addition, VIRS uses an onboard diffuser to view the sun approximately once per month. The VIRS radiometric algorithm uses measurements of these reference sources to provide calibrated spectral radiances for each Earth pixel that it views.

The uncertainties of the VIRS radiances from the visible and SWIR bands are calculated to be 6%. The primary component of these uncertainties, about 5%, comes from the laboratory calibration of the bands. A second component comes from uncertainties in the change of the instrument from its laboratory calibration to the start of on-orbit operations. The uncertainty contribution from the mirror reflectance (system response vs. scan angle) is believed to be small, since the reflectance corrections for these bands are 1% or less. Other instrumental uncertainties are also believed to be small.

The uncertainties for the thermal band radiances are approximately 3%, half those for the visible and SWIR bands. In terms of temperature, the uncertainties are about 2K at 300K. The uncertainty in the radiance from the onboard blackbody, combined with the uncertainty in the linearity of the response of the detectors, accounts for 2/3 of the total. On orbit characterization of response vs. scan angle (scan mirror reflectance) has shown differences of up to 2% from the pre-launch values in the thermal infrared bands located at 10.75 and 11.94 micrometers. However, the use of the on-orbit values does not remove the mirror as a primary source of uncertainty for the VIRS thermal radiances. More detailed information on the VIRS calibration activities may be found in Barnes *et al*, (1999).

3. TRMM Rainfall Algorithms

Rainfall products, their error budgets and the vertical structure of latent heating form the cornerstone of TRMM science. In designing the data systems to generate these products under the very tight budget constraints, it was necessary to minimize the set of products that would satisfy the mission requirements. This section presents an overview of the algorithms deemed critical to the mission success. A summary of these products is presented in Table 4 for reference. The Levels (2, or 3) follow the standard NASA nomenclature. Level 2 consists of the retrieved geophysical parameters at the satellite footprint level, while level 3 products represent either space or time averaged geophysical parameters. Like the Level 1 products, rainfall products follow the version numbers with Version 3 released at launch, Version 4 introduced on Set. 1, 1998 and Version 5 introduced on Oct. 1, 1999. Roughly 2-3 days of data can be reprocessed in 24 hours. Reprocessed products are therefore not available immediately but with some delay depending upon the date the data were collected.

A comprehensive discussion of all the rainfall products is well beyond the scope of this paper. Instead, only the main progress in the rainfall algorithms since launch, and intercomparison between algorithms are presented here. An intercomparison of zonal mean rainfall accumulations for the four major independent rainfall estimates algorithms (Version 4) is presented in Figure 3. These algorithms represent the initial algorithms (Version 4) which are the at-launch algorithms after the initial software errors were corrected. As can be seen from figure 3, there is a wide range between the TMI profiling algorithm and the that of the PR. The following short sections describe the initial improvements to the algorithms that have been undertaken during the first two years along with a comparison of the improved algorithms (Version 5) which became available on Oct. 1, 1999. At the time of this writing, however, only one month of data, February 1998, had been processed with the new algorithms in a test environment. The new results, while probably representative of the other months, have not been examined for time periods other than the one presented here. Rainfall comparisons among the new versions of the algorithms (Version 5) are shown in Figure 4.

3.1 TMI Profiling Algorithm - (TSDIS ref. 2A-12)

The profiling algorithm being used by TMI makes use of the Bayesian methodology to relate the observed multi-channel brightness temperatures to the hydrometeors provided in an a-priori database. This initial database is supplied by non-hydrostatic cumulus-scale cloud models using explicit cloud microphysics. More details can be found in Kummerow *et al.*, (1996). This algorithm was originally developed for the SSM/I and was simply reconfigured for the TMI to take the somewhat different channels and higher spatial resolutions of the TMI into account. The main problem detected with the Version 4 TMI algorithm was the algorithm's inability to correctly identify stratiform rainfall far away from any convection. This problem was made worse by the fact that the cloud numerical simulations all have substantial regions of transition clouds between convective and stratiform clouds. These regions are defined as stratiform in the cloud model by virtue of their small vertical wind

velocity but are very inhomogeneous and thus appear more convective to the passive microwave retrieval algorithm. This problem was corrected by requiring that the spatial inhomogeneity of the TMI also resemble the spatial inhomogeneity of the cloud model profiles found in the database. This modification reduced the rainfall rates in clearly stratiform regimes and was the primary reason for a rainfall reduction between versions 4 and 5. In going from version 4 to version 5, the retrieved latent heating has been temporarily deleted. It was found with version 4 that there were some instabilities in this retrieved heating profiles outside the tropics. It was felt that until the extratropical latent heating profiles could be generated with confidence this product should be set to missing. It is planned to reintroduce the latent heating with version 6 of the algorithm.

3.2 TMI Monthly Rain Mapping Algorithm - (TSDIS ref. 3A-11)

This algorithm produces monthly oceanic rainfall accumulations on a 5°x5° grid. It also originated as an SSM/I algorithm and has been running successfully with that sensor for over 10 years. In this algorithm, the brightness temperatures are considered to be a function of only two variables, the rain rate and the height of the 0°C isotherm (freezing level). The freezing level is associated with the total integrated water vapor content (TIWV) through modeling assumptions – namely that the column water vapor changes from 80% at the surface to saturation at cloud base – assumed to be 500 meters below the freezing level. These assumptions, while weak in the general case, are reasonably robust when restricted to raining conditions. Since the TIWV impacts the 19 and 21 GHz channels very differently whereas the rain impacts them rather similarly, the two channels can be used to solve for the TIWV and, by implication, the freezing level. The rain rate can then be derived using several channel combinations. Since the improved spatial resolution of the TMI can be introduced in a straightforward manner through the beam-filling correction, only minor changes have been made between Versions 4 and 5 of this algorithm. A more detailed description of this

algorithm, and in particular, comparisons between TMI and SSM/I can be found in Chang *et al.*, (1999).

3.3 PR profile - (TSDIS ref. 2A-25)

The rainfall algorithm has undergone a number of changes between version 4 and version 5. Aside from the slight increase in rainfall stemming from the calibration adjustment discussed in Section 2.2.2, the rainfall algorithm has been modified in three additional ways. The first is an improvement of the algorithm for the estimation of the attenuation at the surface. In the new version, uncertainties in both the radar signals and the surface reference are taken into account. The second is the replacement of the DSD measured over Darwin by a more globally justifiable DSD derived from measured DSDs and Z-R relations from various places near the ocean all over the world. The third is the introduction of adjustments in the Z-to-R conversion coefficients that are consistent with the form of the DSD model assumed and the total path attenuation estimate. More details of these procedures can be found in Iguchi *et al.*, (1999). Aside from these algorithm modifications, output data items were slightly changed. Among them the most important change to the user was the removal of the ambiguities between "rain possible" and "rain certain" classifications flowing down from the Level 1 product. In version 4, the algorithm computed rainfall regardless of the rain likelihood, forcing the user to make the determination regarding the likelihood of rainfall. The Version 5 algorithm now makes that determination and sets the rainfall to zero if it determines that rainfall is not probable in a "rain possible" scenario. The net effect of all these changes has been to increase the rainfall derived by the PR by about 15% on the global scale, with roughly a 10% increase in the convective rainfall and roughly a 20% increase in the stratiform rainfall.

3.4 Combined PR/TMI Profiling algorithm - (TSDIS ref. 2B-31)

The guiding principle in the design of the "Day-One" combined algorithms (Version 4) was to merge information from the two sensors into a single retrieval that embodied the strengths of each sensor using a very conservative approach in the beginning. The Version 4 algorithm designed to run at launch used only the 10 GHz channel of the TMI to obtain an independent estimate of the total path attenuation at 13.8 GHz, the frequency of the TRMM Precipitation Radar (PR). Details of this procedure can be found in Haddad *et al.* (1997). This conservative approach has now been refined into a scheme that uses all the TMI channels to construct a solution that best fits all the radar and radiometer data. The version 5 algorithm uses the 85 GHz TMI channels to estimate the amount of ice overlaying the rain, then uses the appropriate parameterized rain-radiances relations (derived from the TMI Profiling Algorithm's a priori database) to find the radar-derived rain profile that best matches the observed radiances. The "best-match" criterion is as in Haddad et al (1997). Details of the rain-radiances relations can be found in Coppens *et al.*, (1999). In addition, the Combined PR/TMI algorithm has also resolved the ambiguity caused by the "rain certain" and "rain possible" conditions introduced by the PR level 1 algorithm.

3.5 TRMM and Other Satellite combination - (TSDIS ref. 3B-42)

The TSDIS algorithm and code for Product 3B-42 is based on the Adjusted GPI (AGPI) technique described by Adler et al. (1994). The technique uses the surface rainfall output from 2A-12, with scaling by the ratios in 3B-31 (both referenced above) to objectively adjust rain rates inferred from geo-IR satellite observations and produce monthly total rain maps for the region of 40°N to 40°S. Specifically, the spatially variable ratio is computed between monthly rain rate averages from coincident 2A-12 (with scaling by 3B-31 ratios) and VIRS infrared data (1B-01), and these monthly ratios are applied to the full 3-hrly geo-IR data set. In version 4, the algorithm produces a pentad (five-day) product on a 1° lat./long grid. The physics of the algorithm has not changed between version 4 and version 5, but there are some

changes in the output product due to changes in the 2B31 algorithm noted above. In addition, the version 5 code generates daily 1°by 1° output files to make it easier for potential users to aggregate data for their individual requirements. Since no additional data were introduced in going from 5- and 30 day products to the daily product, the uncertainty in each daily product has grown proportionally. Figure 5 shows comparisons between the 3B42 product with atoll rain gauge data produced by Morrissey and Greene (1991) as well as the TRMM validation data described in Section 4.

3.6 TRMM and Other Data combination - (TSDIS ref. 3B-43)

The TSDIS algorithm and code for Product 3B-43 are based on the technique described by Huffman et al. (1997). Version 4 combines the TRMM and Other Satellite product (3B-42), TCI (3B-31), and a monthly SSM/I product based on the 2A-12 algorithm (3A-45) into an intermediate multi-satellite product. The scheme is a weighted linear combination done by estimating random errors for each of the input products and then using them to provide weighting by inverse error variance. Version 5 omits the TRMM combined TMI/PR (2B-31 above) and SSM/I products due to concerns about diurnal biases. The final combination with the gauge analysis is the same in both versions, and again uses a linear combination with inverse error variance weighting.

3.7 New products developed by TSDIS

TSDIS generates the TRMM standard products and is responsible for distributing data to the TRMM algorithm development team. The Goddard DAAC (Distributed Active Archive Center) performs the broader distribution of data. The interface to both data systems is web based and both can be accessed from the TRMM Web site http://trmm.gsfc.nasa.gov. In Japan, TRMM scientists and associated researchers can access these same products through the NASDA data system accessible via: http://www.eorc.nasda.go.jp/TRMM/.

For convenience of the algorithm development team, TSDIS also routinely produces subsets of the data products that provide data only over the 10 designated ground validation sites and some additional sites desired by the science team. These subsets have the same format as the regular products but are much smaller. The Goddard DAAC is also making these subsets available to its general users. TSDIS also has a limited capability of producing special subsets for the algorithm development team that can cover regions of the globe other than the TRMM ground validation sites. Such subsets are produced at the request of an algorithm developer for the area and time period that they specify.

Because of the early success for the data system, TSDIS has been able to provide expanded product capabilities. In July 1998, TSDIS began generating near real-time data products. The products are the same as the official products described above, but the output data have been reduced drastically to only those parameters that might be of use to the real-time users. This includes surface rainfall and 20 (instead of 80) layers of the PR vertical structure. Unlike the normal data stream which is generated on an orbit-by-orbit basis, the real-time data varies in size depending upon TRMM contact with the Data Relay Satellite. Near real-time data are generally available within 3 hours of collection of the oldest bit in the data stream.

In addition to the near-real time data products, TSDIS has also begun distributing gridded surface rainfall data. Global data at 0.5° resolution, as well as land data over South America and Africa are available at 0.1° resolution. Both datasets contain the rainfall and convective fraction of rain from the TMI, PR and combined TMI/PR algorithms. The files are produced daily and are written in plain text format for ease of use. The data are written into the grid box that had a TRMM overpass, recording both the time of the overpass of the first pixel in that grid box, the rainfall parameters and the necessary statistics of observations within the grid box to allow for later reconstruction of rainfall accumulations. Further reference on obtaining any of these products is available from the TSDIS web site.

4. Validation Efforts During the First Two Flight Years

The validation efforts of TRMM are separated into two categories. The first is the routine validation of rainfall products produced by a number of cooperative radar sites. The second consists of an aggressive schedule of Field Experiments around the globe designed to physically validate many of the assumptions both the spaceborne as well as the ground based instrument algorithms.

To increase credibility of the TRMM products it is necessary to conduct special measurements at and near the Earth's surface. The TRMM Ground Validation (GV) program is composed of two primary efforts: climatological validation and physical validation. General objectives are to obtain an improved understanding of the physical processes associated with clouds and precipitation that ultimately lead to improvements in their remote sensing and representation in numerical models. In climatological validation, standard products are produced from various sites that have one or more calibrated radars and a network of regularly maintained rain gauges. The objective is to provide independent validation of the satellite products at select locations.

4.1 Climatological Validation

Table 5 describes basic characteristics for the four primary validation sites. The primary sites are described in detail on the TRMM web site under "validation". Radar and rain gauge data are provided on a continuous, routine basis to Goddard, from which standard products are generated. The exception is Darwin, in which data are received only during the 5-6 month long wet season. Products from five additional special climatology sites (Guam, Taiwan, Brazil, Israel, and Thailand) during select, 3-6 month periods of interest to TRMM are currently being generated by investigators at their home institutions.

Data quality is a major challenge in climatological validation. The rainfall products are only as good as the quality of the radar and rain gauge data. Raw radar data are contaminated by returns from non-meteorological targets (bugs, birds, the surface [anomalous propagation], chaff, wildfires). The current quality control algorithm requires an analyst to vary adjustable parameters in order to remove these echoes. Rain gauge data are also edited by comparing temporal and spatial correlations with radar-derived rainfall estimates (using $Z=300*R^{1.4}$) over the locations of the gauges. An automated procedure was developed that determines which of the gauges pass this quality control step (Amitai, 1999; Marks *et al.,* 1999), and the algorithm performed very well when compared with manual inspection of the merged gauge-radar data. Hereafter those gauges that pass this quality control step will be referred to as "good" gauges. Monthly rainfall estimates improve by up to 50 percent when quality control measures are applied to the radar and gauge data sets (Kulie et al., 1999: Robinson et al., 1999; Marks et al., 1999).

Rain maps are generated from each of the primary sites following Steiner et al. (1995). Radar-derived rainfall estimates (using $Z=300*R^{1.4}$) over the locations of the good gauges are adjusted by 7-min averaged rain rates measured by these gauges. A final relationship is derived, $Z=A*R^{1.4}$, in which $A=300*(\mathbf{R/G})^{1.4}$, $\mathbf{R}$ is the total rainfall estimated by the radar over the good gauges, and $\mathbf{G}$ is the accumulated rainfall measured by the good gauges. This bulk adjustment is applied separately for rainfall classifications, resulting in convective and stratiform ZR relationships, $A_{conv}*R^{1.4}$ and $A_{strat}* R^{1.4}$, respectively. This bulk adjustment is applied to a month of data from each site. If the total accumulation of rainfall from the sum of the good gauges is less than 250 mm, then the procedure is applied to several months of data for that site, in order to avoid numerical instabilities in the procedure.

A comparison of TRMM products with the GV rain maps was shown in Figure 5b. The monthly rain estimates agree to within 20% is also the uncertainty among the TRMM algorithms. Because surface radars require occasional maintenance and repair, they cannot operate continuously like satellites. A more definitive comparison is underway by taking a subset of the satellite measurements matched to when the radars are operating, in which the monthly GV and satellite rainfall estimates are expected to agree within 15%. Like the satellite products, the Climatological validation products also use Version numbers to track continuously improving algorithms and methods. They are, however, not tied to the satellite Versions to avoid the need to validate with products that are themselves evolving. At the time of this writing, Version 3 was in effect for the validation products.

4.2 Physical Validation

Table 6 lists the five different field experiments that were conducted during the first two years of the mission. These data sets will be used to evaluate the physical assumptions made by rainfall algorithms, initialize and validate the cloud resolving models, test latent heating retrievals from the TRMM observables, and evaluate methods of estimating rainfall and latent heating from ground based radars. In addition to this basic set of objectives, the field experiments were designed as a group in order to insure that the specific observations could also be compared between experiments in order to gain some insight into the regional dependence of any findings. A number of measurements are therefore common to all experiments.

The core of all experiments consisted of a pair of Doppler radars needed to obtain the vertical air motions that are critical to independently verify the latent heating profiles associated with precipitation. Similarly, all experiments had significant levels of meteorological soundings in order to initialize cloud scale models that provide the input for TRMM based latent heating estimates. Area-averaged divergence and budgets of heat and moisture will be

derived from radiosonde networks in TRMM-LBA and KWAJEX. Comparisons between these various methods for arriving at the latent heating profiles must ultimately form the basis for any latent heating profiles derived from the satellite.

The other objective of the Field Experiments is to validate the physical assumptions made by the TRMM retrieval algorithms. It is vital that the assumptions made by the TRMM sensor, as well as ground based algorithms be carefully checked in order to gain confidence that we not only have the right answer, but have it for the right reason. Foremost among these is verification that the TRMM radar is using statistically appropriate drop size distributions (DSD). To meet this goal, all experiments contained at least one aircraft capable of measuring DSD in situ plus at least one aircraft capable of simulating the TRMM observations. The latter is important in order to insure that enough samples are obtained during each campaign. There were also excellent in situ measurements of ice, which documented the variations in habits and their particle size distributions as functions of temperature (height) in different parts of the storms also coordinated with at least one aircraft capable of simulating the TRMM observations. This important information should lead to improvements in the retrievals and in the cloud models.

5. Early Applications

Beginning with version 5, the independent TRMM rainfall products achieved agreement among themselves as well as ground observations that are all within 20%. While much work remains to be done to continue to improve space- and ground-based rainfall estimates, and derive credible uncertainty estimates, the greater confidence in TRMM based products, and their SSM/I derivatives has already had a significant impact upon a number of applications. Some of the ongoing efforts are described briefly described below.

5.1 Tropical Cyclones

The ability to forecast intensity changes in tropical cyclones has shown little progress in the past two decades. With more than 84 Tropical Cyclones sampled in the first 13 months of operations, TRMM offers unique opportunities to identify both accelerators and brakes upon intensity. Within a few days after launch in November 1997, TRMM witnessed the birth of twin typhoons. An equatorial westerly wind burst flared up 2000 km southwest of Hawaii. Paka formed in the Northern Hemisphere and Pam in the Southern. At first Paka remained weak, until on December 10 a huge convective burst occurred (Figure 6). In the Figure, the upper left panel shows the geosynchronous view. The large round white area is the top of one of the early "hot towers". The upper right panel shows the TRMM radar superimposed on the geosynchronous image, while the lower left panel is the 85 GHz image from the TRMM Microwave Imager (TMI). Both the radar and the passive microwave show a clear eye, which was hidden on the geosynchronous image. The lower right shows a radar cross section from A to B on the radar image above. The very high tower leans slightly inward toward the eye. Other radar cross sections show cloud material extruding from the cloud into the eye and almost surely sinking. The convective burst is associated with Paka's first rapid intensity increase from about 27 m s-1 to above 50 m s-1 on December 11. Paka was a mature Typhoon until December 22, crossing the entire North Pacific. It caused great damage in Guam and became a Supertyphoon shortly thereafter. The first rapid deepening has been studied and related to a combination of the convective burst's carrying up high energy air (Halverson *et al.*, 1999) and the storm core moving over warmer water (Rodgers *et al.*, 1999).

The TRMM PR and TMI images of tropical cyclones are especially noteworthy for their potential operational use as well as their obvious research applications. The TRMM radar data can be displayed in plan view at a number of altitudes or in vertical cross-section format. The 250 meter vertical resolution of the PR data are much more detailed than can be obtained

from operational radars except at very close range. Even the 85 GHz images alone have demonstrated their ability to distinguish between average and intense eyewall convection, as in this recent overpass of Category 4 Hurricane Floyd approaching the Bahamas (Fig 2). In fact, for the past two hurricane seasons, the Navy has provided TRMM as well as SSM/I images in near-real time on their tropical cyclone home page http://kauai.nrlmry.navy.mil:80/sat-bin/tc_home and the operational agencies are making increasing use of these images.

5.2 Improving assimilated global data sets using TMI rainfall and Total Precipitable Water (TPW) observations

The precipitation and total precipitable water (TPW) estimates derived from the TMI have proven to be effective for improving assimilated data sets. Conventional global analyses currently contain order-one errors in primary hydrological fields such as precipitation and evaporation, especially in the tropics. The TMI-derived rainfall and TPW estimates may be used to constrain these fields to produce a global analysis useful for understanding the role of tropical convection in global climate variability. Pilot studies carried out at the NASA Goddard Space Flight Center have shown that assimilating the 6-hr averaged TMI surface precipitation and TPW estimates improves not only the primary hydrological fields but also key climate parameters such as clouds and radiation in the analysis produced by the Goddard Earth Observing System (GEOS) data assimilation system (DAS). This section highlights some of the benefits of using TMI rainfall and TPW data in global data assimilation.

The precipitation and TPW assimilation algorithm used in the GEOS DAS is based on a 6-hr time integration of a column version of the GEOS DAS, which minimizes the least-square differences between the observed TPW and rain rates and those generated by the column model over a 6-hr analysis window. This "1+1" dimensional scheme, in its generalization to four dimensions, is related to the standard 4D variational assimilation but employs moisture

analysis increments instead of the initial condition as the control variable (see Hou et al., 1999, for details of the algorithm).

In assimilation experiments in which the 6-hr averaged r rainfall (Kummerow *et al.* 1996) and TPW retrievals (Wentz, 1999) are assumed to be "perfect" relative to the model's first guess, the impact of these data on the GEOS analysis is to reduce the state-dependent systematic errors in tropical precipitation and TPW fields. Since clouds and radiation are directly affected by moist convection, the improved hydrological cycle, in turn, provides better estimates of atmospheric energetics. This is evident in the improved Outgoing Longwave Radiation (OLR) and Outgoing Shortwave Radiation (OSR) as verified against independent measurements provided by the Clouds and the Earth's Radiant Energy System (CERES) instruments aboard the TRMM satellite.

Figure 7 summarizes the impact of TMI rainfall and TPW assimilation on the monthly-mean precipitation, TPW, OLR, and OSR in the tropics for January 1998. These monthly plots are based on assimilation results sampled with the same spatial and temporal resolution as the satellite data sets used for verification. The left panel shows time-mean spatial errors in the these fields in the GEOS control assimilation. The right panel shows the corresponding errors in an assimilation that incorporates the TMI rainfall and TPW observations. The monthly-mean spatial biases and error standard deviations are significantly reduced in most fields. The two apparent exceptions are the biases in the tropical-mean precipitation and OLR. The slightly larger precipitation bias reflects that the rainfall assimilation algorithm is more effective in reducing than enhancing precipitation, but the difference of 0.6 mm day-1 is within observation uncertainties. The apparent increase in the OLR bias is due to the virtual elimination of the negative OLR bias associated with precipitation, leaving tropical-mean bias dominated by the positive (but reduced) bias in the rain-free regions. In the GEOS

analysis the OSR errors are dominated by errors in the clouds. The improved OSR is therefore indicative of improved cloud patterns.

5.3 Improving tropical precipitation forecasts from a multi-analysis super-ensemble

This study makes use of the notion of a multi-model super-ensemble developed by Krishnamurti et. al. (1999 a, b) for the improvement of seasonal climate, global weather, and hurricane track and intensity forecasts. Those two papers show that super-ensemble forecasts are invariably superior in skill to the individual multi-models. This same notion is being used here for demonstrating the large impact of TRMM data sets on global prediction of rainfall. The procedure begins with what are called multi-analysis forecasts of rainfall. The multi-analysis comes from the use of different rain rate algorithms for the initialization (using physical initialization of rain rates, Krishnamurti, et al. 1991) for several different rain rate algorithms. Next, a total of 180 experiments are run with the FSU global spectral model at the resolution T126 (roughly 80km resolution) with these several options. Each experiment entails physical initialization of the observed rain (as measured by the different algorithms) and is followed by a three-day global forecast. These experimental runs are then compared to an "observed" rainfall field which is derived from the most credible source (the TRMM algorithms in this case). This entire data generated from the multi-analysis based forecasts and these 'observed' best estimates are regressed to obtain weights via multiple regression for each of these forecasts weighed against the best 'observed' measures.

The next step in this exercise calls for a set of 30 new forecasts for a new period. Here the previously generated statistics (i.e. weights) are used along with the new multi-analysis forecasts to design superensemble forecasts. Three day forecasts have been shown to have very high forecast skills compared to the direct forecasts from the use of the physical initialization of a single run with a single rain rate algorithm. These improvements can be measured against past performance, when only physical initialization was used. Figure 8

illustrates a past skill, i.e. the correlation of predicted and observed rainfall, plotted against the forecast days. This illustration is based on Treadon (1996). The Figure shows that there is a very high nowcasting skill in these correlations, i.e. of the order of 0.9. This was a feature of physical initialization. The forecast skill degrades to 0.6 by day 1 of forecast. That skill degrades further by days 2 and 3 to values, such as 0.5 and 0.45 (respectively). Using the superensemble approach, one is able to improve those numbers when the TRMM/SSM/I -based rain rates are used as a benchmark for the definition of the superensemble statistics and the forecast verification. Figure 9 illustrates the TRMM-based forecast skills over several selected regions of the globe. The major impact of TRMM towards improving regional short-range forecasts can be noted when compared to results obtained in 1996. Finally, Figure 10 shows examples of rainfall forecasts on day 3 of forecasts, compared to the observed TRMM-based estimates at correlation levels of around 0.7 at day 3. This is a major accomplishment from the use of TRMM satellite data. Such forecasts can only improve if the global rainfall is further improved with additional sampling.

6. Summary and Next Steps

In this paper, we have summarized the latest progress in calibrating TRMM and achieving consistency among TRMM rainfall estimates with each other and ground based measurements. We have also shown the significant impact that high quality spaceborne radar and radiometer measurements have on the understanding of precipitation physics, on other related atmospheric phenomena, and on the improvement that can be achieved in data assimilation for atmospheric prediction. There are a number of other ongoing research efforts within the TRMM project which are just as important. These include the modeling of ocean surface temperature anomalies due to fresh water fluxes, the application of TRMM rainfall for land hydrology analysis and modeling, the investigation of intense rain systems on atmospheric electricity generation plus feedbacks on rain microphysics from intensifying

electrical fields, and determining the rate of atmospheric overturning during the 1997-98 El Niño. Notably, the latter research may begin to shed light on the potential impacts on regional rainfall that could stem from a global warming process.

However, TRMM alone cannot solve all problems associated with precipitation. The TRMM satellite's major drawbacks are its limited global sampling and its finite mission lifetime. TRMM does not provide measurements outside of the tropics (35°N - 35°S), and its lifetime is only expected to be 3-5 years due to its low orbit. Moreover, the sampling frequency at any given point by the TRMM radiometer is limited to approximately 1 sample every 15 hrs while the TRMM radar is limited to approximately 1 sample every 50 hrs (depending upon the latitude of the sample). Although rainfall uncertainties due to insufficient temporal sampling can be studied and quantified using the TRMM retrievals in conjunction with ground-based validation data, they cannot be overcome based on a single, Earth orbiting satellite. Thus, while TRMM's attributes are many, TRMM rainfall uncertainties are dominated by sampling error. The consequence of a short satellite lifetime and limited sampling is to preclude detecting subtle changes in the rainfall distribution and its associated diabatic heating field that might result from a slowly changing climate. Notably, since TRMM was never designed to address such a challenges, NASA and NASDA are now in the initial planning phases of a new mission called the Global Precipitation Mission (GPM), tentatively planned for launch in 2006.

The GPM concept will address climate-rainfall variability and has been formulated with two components. A single primary satellite will be an enhanced, TRMM-like satellite that can quantify the 3-dimensional spatial distribution of precipitation and the associated latent heat release. This "core" platform will carry a dual frequency rain radar plus a multi-channel, polarized passive microwave radiometer akin to TMI. By use of two radar frequencies, it will be possible to determine the first moment of the drop size distribution (i.e., the DSD

mode) and thus rainfall rates that will exceed the quality of standard ground-based weather radars. By merging the radiometer measurements with the dual frequency radar measurements in a combined algorithm formulation, it may be possible to obtain information indirectly on the second moment of the DSD (i.e., the distribution spread). The radiometer brightness temperatures, as is the case for TRMM, also provide further insights into cloud properties and cloud processes beyond that given by radar reflectivities alone, plus help transfer insights into the wider radiometer swath regions not observed by the radar, as well as the swaths of complementary satellites that form the second component of the GPM concept.

The second mission component of GPM consists of a number of small radiometer satellites (or microsats) flown in a constellation configuration with the primary satellite, providing the necessary diurnal sampling needed in forcing hydrometeorological models and error reductions in time-averaged rainfall estimates to levels below those intrinsic to hydrologic and atmospheric models. Rain measuring is obtained from a microsat by the primary satellite "training" the microsat radiometer to retrieve rainfall statistically normalized to the near contiguous "core" satellite retrievals. With a total of 8 constellation radiometers, which could consist of a mixture of microsats and various operational satellites carrying passive microwave radiometers (such as SSM/I on DMSP and AMSR on ADEOS II or EOS-PM), a sampling frequency of 3 hours would be achieved. This reduces sampling uncertainties to below 10% for daily rainfall accumulations. As demonstrated with ongoing research related to TRMM, such measurements will have significant positive impacts on prognostic model data assimilation and weather forecasting skill, as well as on hydrological applications that require near continuous sampling.

Because the microsat drones must be small, lightweight, and economical on energy consumption, a new lightweight radiometer is currently being demonstrated by NASA to meet the needs of the GPM. This will mean the primary cost drivers for the microsats will only be the buses and launch vehicle(s). In addition, NASA is conducting a design study of a

dual frequency rain radar with polarization and Doppler coherency, an instrument which could eventually replace the initial radar system on future missions. This design would, in theory, enable direct retrieval of the first three moments of the DSD (i.e., the mode, spread, and skew associated with the large drop tail), Also, through multi-parameter techniques, such a radar could address the important problems of determining the physical properties of precipitating ice (i.e., size distributions, volume cross sections, particle shapes and habits, canting angle distributions), as well as explicitly differentiating ice from supercooled water.

Acknowledgments

Any successful program such as TRMM typically owes its success to countless individuals who, with their foresight and dedication, continuously steer a mission in the right direction. Through their efforts, TRMM has been continuously able to not only meet, but to exceed most of the science and engineering goals set forth for this mission. The authors would therefore like to thank, in addition to NASA and NASDA, which made the mission possible, all the individuals that helped build the satellite and data systems, all the individuals responsible for its safe operations, and all the scientists around the globe for their dedicated efforts.

REFERENCES

Adler, R. F., G. J. Huffman, and P. R. Keehn, 1994: Global tropical rain estimates from microwave-adjusted geosynchronous IR data. *Remote Sensing Reviews*, **11**, 125-152.

Amitai, E., 1999: Dependence of Z-R Relations on the rain type classification scheme. Preprints, *29th International Conference on Radar Meteorology*, Montreal, Canada, American Meteorological Society, 636-639.

Barnes, R. A., W. L. Barnes, C-H. Lyu and J. M. Gales, 1999: An Overview of the VIRS Radiometric Calibration Algorithm. *J. Atmos. Oceanic Tech.*, accepted.

Chang, A.T.C., L. S. Chiu, C. Kummerow, and J. Meng, 1999: First Results of the TRMM Microwave Imager (TMI) Monthly Oceanic Rain Rate: Comparison with SSM/I. *Geophys. Res. Letters*, **26**, 2379-2382.

Coppens, D., Z. Haddad and E. Im, 1999: Estimating the uncertainty in passive-microwave rain retrievals. *J. Atmos. Oceanic Tech*, submitted.

Christian, H.J., R.J. Blakeslee, and S.J. Goodman, 1992: Lightning imaging sensor (LIS) for the earth observing system. NASA TM-4350, Available from Center for Aerospace Information, P.O. Box 8757, Baltimore Washington International Airport, Baltimore, MD 21240, 44.

Haddad, Z. S., E.A.Smith, C.D.Kummerow, T.Iguchi, M.R.Farrar, S.L.Durden, M.Alves and W.S.Olson, 1997: The TRMM `Day-1' radar/radiometer combined rain-profiling algorithm. *J. Met. Soc. Japan* 75 (4), 799-809.

Halverson, J. B., Pierce, H., Simpson, J., Morales, C., Rodgers, E.B., Stewart, S. and Iguchi, T., 1999: First TRMM Satellite observations of a deep convective burst in Supertyphoon PAKA (1997). *23rd Conf. On Trop. Meteor. and Hurricanes*, American Meteorological Society, Dallas, TX, 997-1001.

Huffman, G.J., R.F. Adler, P. Arkin, A. Chang, R. Ferraro, A. Gruber, J. Janowiak, A. McNab, B. Rudolf, U. Schneider, 1997: The Global Precipitation Climatology Project (GPCP) Version 1 Data Set. *Bull. Amer. Meteor. Soc.*, **78**, 5-20.

Hou, A.Y., D.V. Ledvina, A.M. da Silva, S.Q. Zhang, J. Joiner, R.M. Atlas, G.J. Huffman, and C.D. Kummerow, 1999: Assimilation of SSM/I-derived surface rainfall and total precipitable water for improving the GEOS analysis for climate studies. *Mon Wea. Rev.*, in press.

Iguchi, T., Kozu, T., Meneghini, R., Awaka, J. and Okamoto, K., 1998: Preliminary results of rain profiling with the TRMM precipitation radar. *Proc. 8th URSI Com F Triennial Open Symposium* . "Wave Propagation and Remote Sensing", Aveiro Portugal, 147-150.

Krishnamurti, T.N., 1999a: Improved skills for weather and seasonal climate forecasts from multi-model superensemble. *SCIENCE*, submitted.

Krishnamurti, T.N., C.M. Kishtawal, David Bachiochi, Zhan Zhang, Timothy Larow, Eric Williford, Sulochana Gadgil, and Sajani Surendran, 1999b: Multi-Model Superensemble

Forecasts for Weather and Seasonal Climate. *Meteorology and Atmospheric Physics*, submitted.

Krishnamurti, T.N., J. Xue, H.S. Bedi, K. Ingles and D. Oosterhof, 1991: Physical initialization for numerical weather prediction over the tropics. *Tellus*, **43AB**, 53-81.

Kulie, M. S., Robinson, M., Marks, D.A., Ferrier, B.S., Rosenfeld, D. and Wolff, D.B., 1999: Operational processing of ground validation data for the Tropical Rainfall Measuring Mission. Preprints, *29th International Conference on Radar Meteorology*, Montreal, Canada, American Meteorological Society, 736-739.

Kummerow, C., W.S. Olson, and L. Giglio, 1996: A simplified scheme for obtaining precipitation and vertical hydrometer profiles from passive microwave sensors. *IEEE Trans. Geosci. Remote Sens.*, **34**, 1213-1232.

Kummerow, C., W. Barnes, T. Kozu, J. Shiue, and J. Simpson, 1998: The Tropical Rainfall Measuring Mission (TRMM) Sensor Package. *J. Atmos. and Ocean Tech..*, **15**, 808-816.

Lee, R. B. Barkstron, B. R, Bitting, H. C. Crommelynck, D.A.H., Paden, J., Pandey, D.K., Priestley, K. J., Smith, G. L., Thomas, S., Thornhill, K.L., and Wilson, R.S., 1998: Prelaunch calibrations of the CERES TRMM and EOS-AM1 spacecraft thermistor bolometer sensors. *IEEE Trans. Geo. and Rem. Sens.*, **36**, 1173-1185.

Marks, D. A., Kulie, M.S., Robinson, M., Ferrier, B.S., and Amitai, E., 1999: Standard reference rainfall products used in Tropical Rainfall Measuring Mission ground validation efforts. Preprints, *29th International Conference on Radar Meteorology*, Montreal, Canada, American Meteorological Society, 744-747.

R. Meneghini, R., T. Kozu, H. Kumagai, and W.C. Boncyk, 1992: A study of rain estimation methods from space using dual-wavelength radar measurements at near-nadir incidence over ocean. *J. Atmos. Oceanic Technol.*, **9**, 364-382.

Morrissey, M.L., and J. S. Green, 1991: The Pacific Atoll Raingauge Data Set. Planetary Geosci. Div. Contrib. 648, Univ. of Hawaii, Honolulu, HI, 45 pp.

Robinson, M., Marks, D.A., Kulie, M.S. and Ferrier, B.S., 1999: Seasonal characteristics of non-meteorological radar reflectivity return in East Central Florida and their impact on TRMM Ground Validation. Preprints, *29th International Conference on Radar Meteorology*, Montreal, Canada, American Meteorological Society,740-743.

Rodgers, E.B., Halverson, J.B., Olson, W. and Pierce, H., 1999: Tropical Cyclone PAKA's initial explosive development (10-12 December, 1997). *23rd Conf. On Trop. Meteor.* 471-474.

Rosenfeld, D., 1999: TRMM Observed First Direct Evidence of Smoke from Forest Fires Inhibiting Rainfall, *Geophys. Res. Letters*, submitted.

Shin, K.-S, and G.R. North, 1988: Sampling error study for rainfall estimates by satellite using a stochastic model. *J. Appl. Meteor.* **27**, 1218-1231.

Simpson, J. (Ed.), 1988: TRMM—A Satellite Mission to Measure Tropical Rainfall. Report of the Science Steering Group. NASA Publications, U.S. Gov't Printing Office. Washington, D.C. 94 pp.

Steiner, M., Houze, R.A., Jr. and Yuter, S.E., 1995: Climatological characterization of three-dimensional storm structure from operational radar and rain gauge data. *J. Appl. Meteor.*, **34**, 1978-2007.

Takayabu, Y. N., T. Iguchi, N. Kachi, A. Shibata, and H. Kanzawa, 1999: Abrupt termination of the 1997-98 El Nino in response to a Maddan-Julian oscillation. *Nature*, submitted.

Treadon R.E., 1996: Physical initialization in the NMC global data assimilation system. *Meteorol. Atmos. Phys.*, **60** (1-3), 57-86.

Viltard, N., C. Kummerow, W. S. Olson and Y. Hong, 1999: Combined use of the Radar and Radiometer of TRMM to Estimate the Influence of Drop Size Distributions on Rain Retrievals. *J. Appl. Meteor.*, submitted.

Wentz, F., 1999: Description of TMI and SSM/I data products available online from http://www.ssmi.com. Remote Sensing Systems, Santa Rosa, Calif.

Figure Captions

Figure 1 Regression lines of TMI minus SSM/I T_A difference (ΔT_A) and SSM/I T_A. for common SSM/I and TMI channels.

Figure 2: Hurricane Floyd as captured by the TRMM PR superimposed over GOES image. PR corss section AB and CD are shown in insets.

Figure 3: Monthly, zonally averaged mean rainfall derived from 4 independent TRMM rainfall algorithms using the initially corrected at-launch algorithm version (Version 4)

Figure 4: Monthly, zonally averaged mean rainfall derived from 4 independent TRMM rainfall algorithms after the first substantial improvement cycle was implemented on Oct. 1, 1999 (Version 5).

Figure 5: Comparison of TRMM adjusted IR rainfall estimates. (a) comparison with atoll rain gauge data. (b) comparison with TRMM ground based radar rainfall products.

Figure 6: Geosynchronous and TRMM imagery of early stage of STY Paka in the North Pacific at 0532 UTC on Dec 10, 1997. The upper left is GMS Geosynchronous image alone. Note bright convective burst near storm center. The upper right superimposes the TRMM radar image on the geosynchronous image. The lower left shows the TMI image superposed on the GMS and the lower right is a precipitation radar profile between A and B.

Figure 7: NASA GEOS assimilation results with and without TMI observations for January 1998. The panel on the left shows errors in the monthly-mean tropical precipitation, total precipitable water, outgoing longwave radiation, and outgoing shortwave radiation in the

GEOS control assimilation. The panel on the right shows the impact of assimilating TMI rainfall and TPW observations on these fields. The percentage changes relative to errors in the GEOS control are given in parentheses. See text for discussions of bias values accompanied by an asterisk.

Figure. 8: Skill of precipitation forecasts over global Tropics, (30S to 30N) based on point correlation, Treadon (1996). Abscissa shows dates of forecast. Different curves show the correlation of NCEP operational model, results based on physical initialization with two options (with and without the improvement of surface fluxes).

Figure. 9: Skill of the precipitation forecasts over Africa (0 to 60E) for: control forecast; physical initialization using TRMM data only; superensemble forecasts where the TRMM plus SSM/I rain rates are used as a benchmark. Abscissa denotes days of forecast..

Figure 10: Comparison (in units mm day $^{-1}$) of observed estimates (based on TRMM and SSM/I) and the day 3 forecast from the superensemble. (a) Global Tropics; (b) Africa; (c) Tropical Americas.

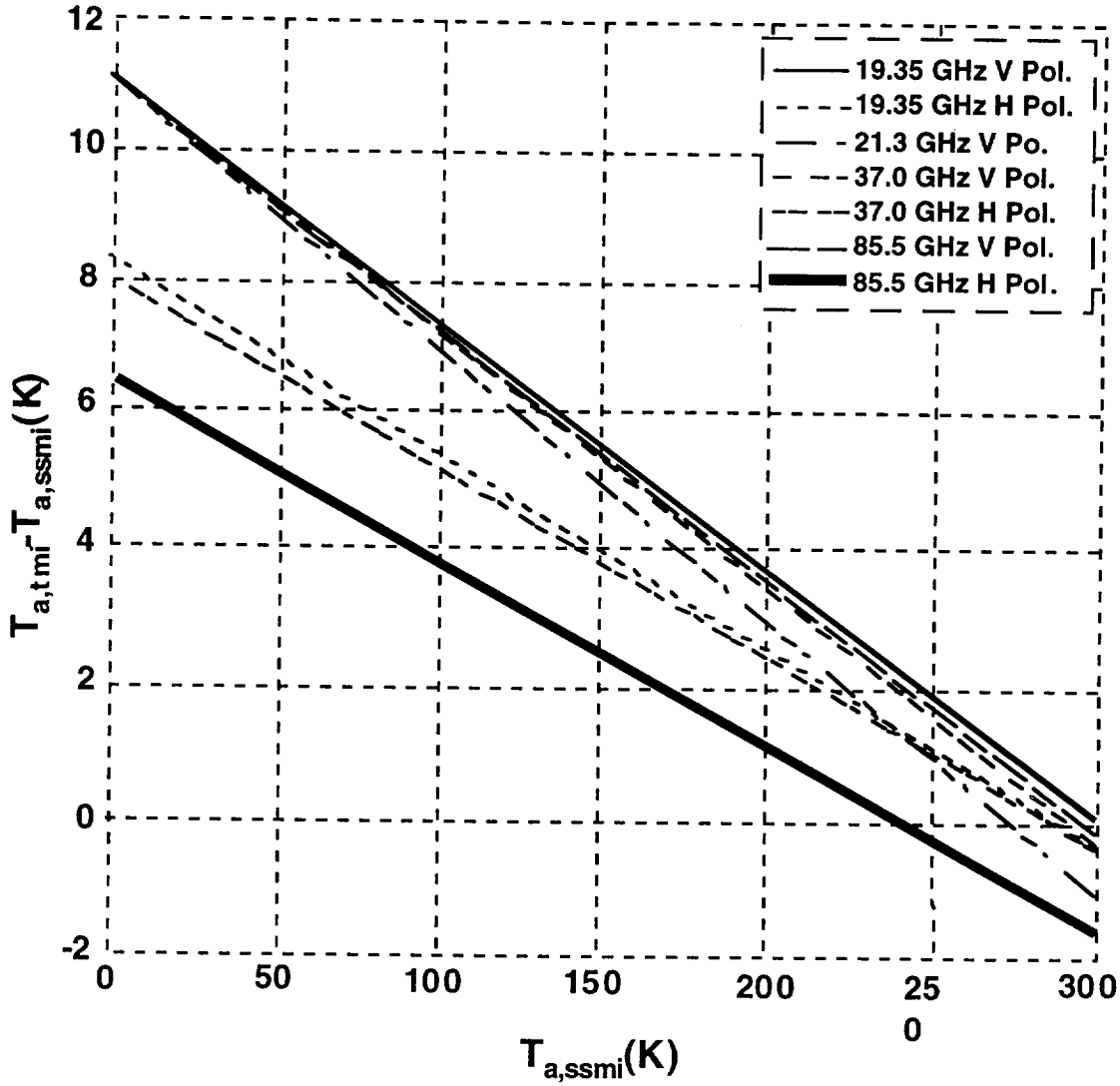
12
10
8
6
4
2
0
-2
0
50
100
150
200
250
300
$T_{a,tmi}$-$T_{a,ssmi}$(K)
$T_{a,ssmi}$(K)
19.35 GHz V Pol.
19.35 GHz H Pol.
21.3 GHz V Po.
37.0 GHz V Pol.
37.0 GHz H Pol.
85.5 GHz V Pol.
85.5 GHz H Pol.

Figure 1

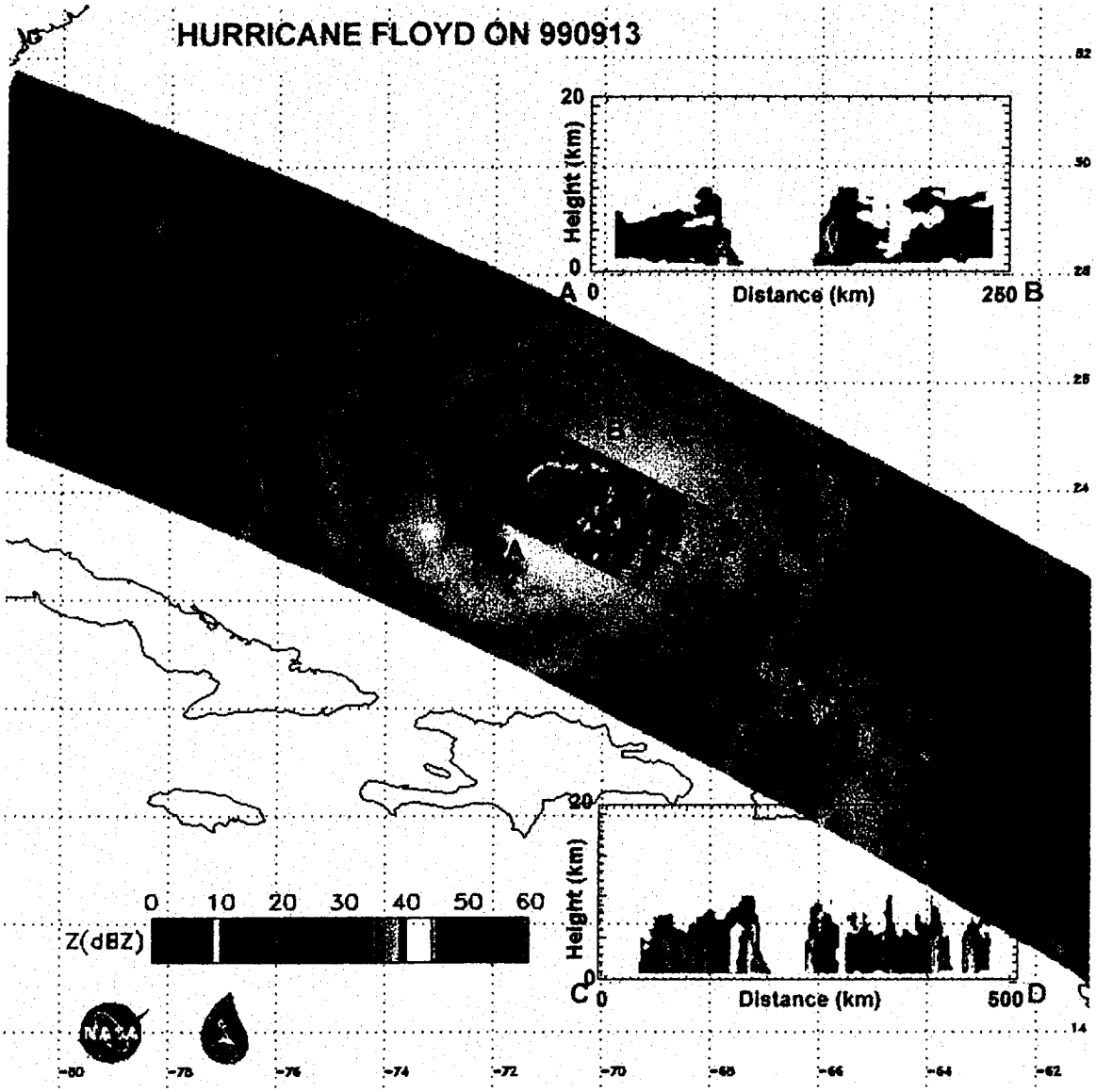
HURRICANE FLOYD ON 990913
Height (km)
20
0
A
0
Distance (km)
250
B
Height (km)
20
0
C
0
Distance (km)
500
D
0 10 20 30 40 50 60
Z(dBZ)
NASA

Figure 2

Feb., 1998 (TSDIS version 4)

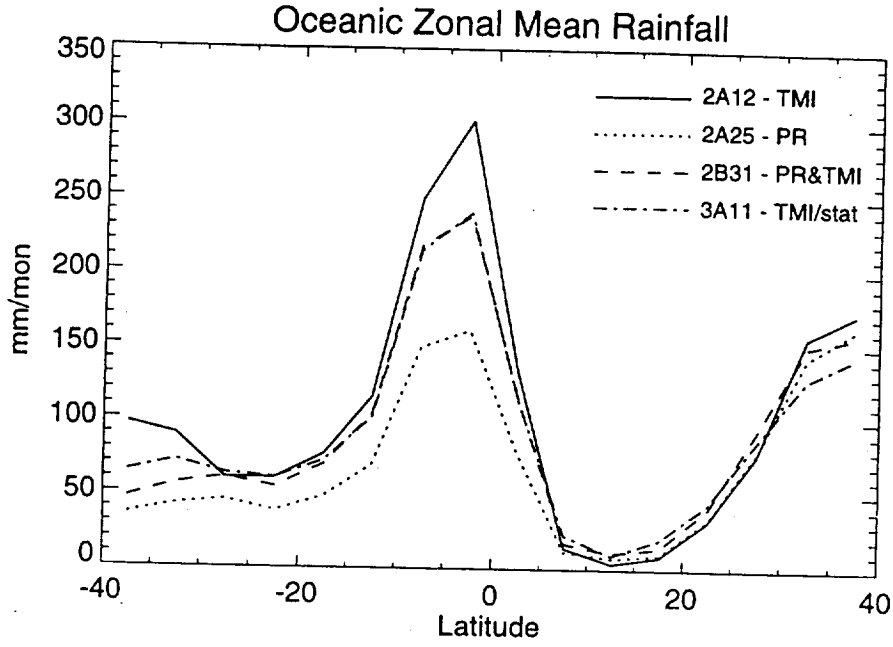

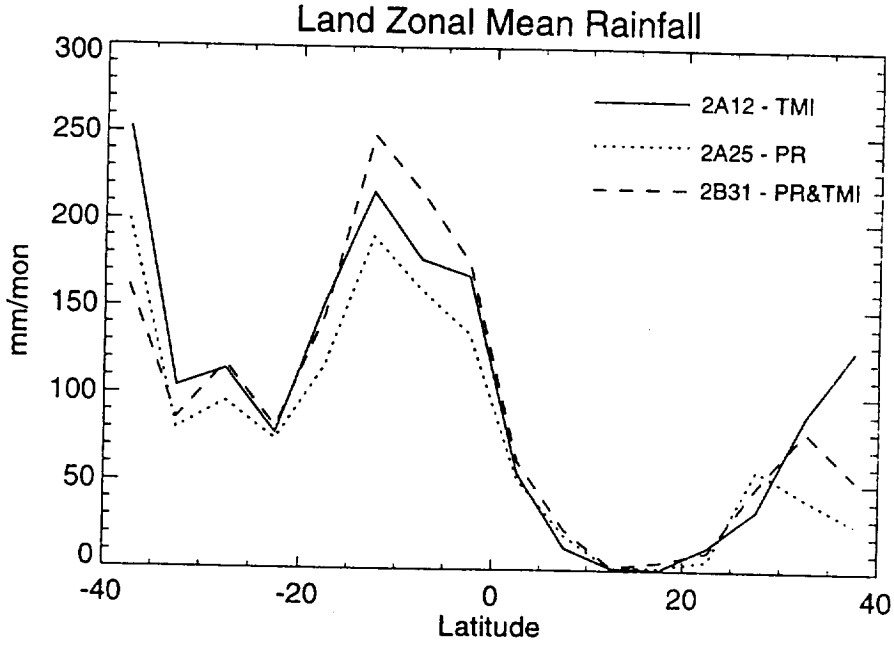

Figure 3

Feb., 1998 (TSDIS version 5)

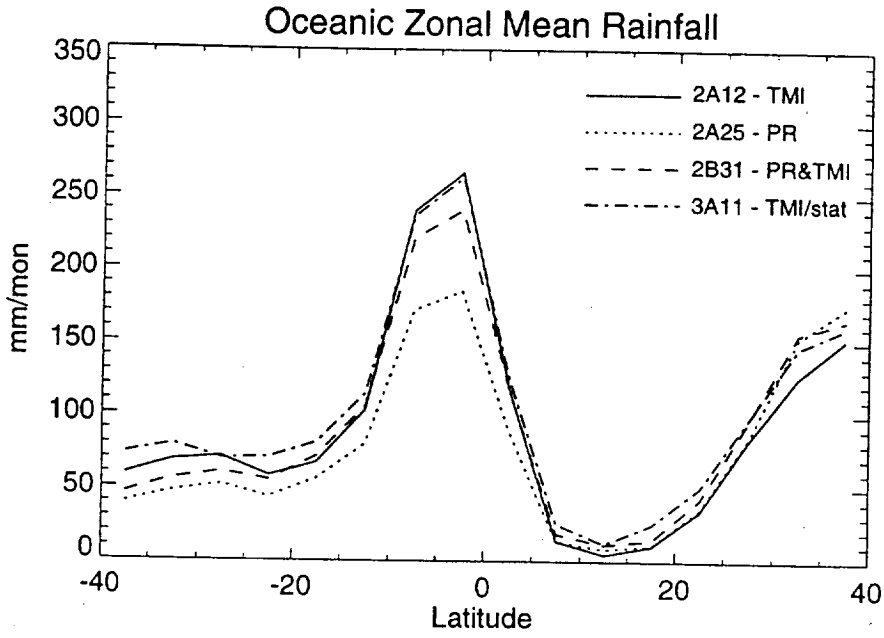

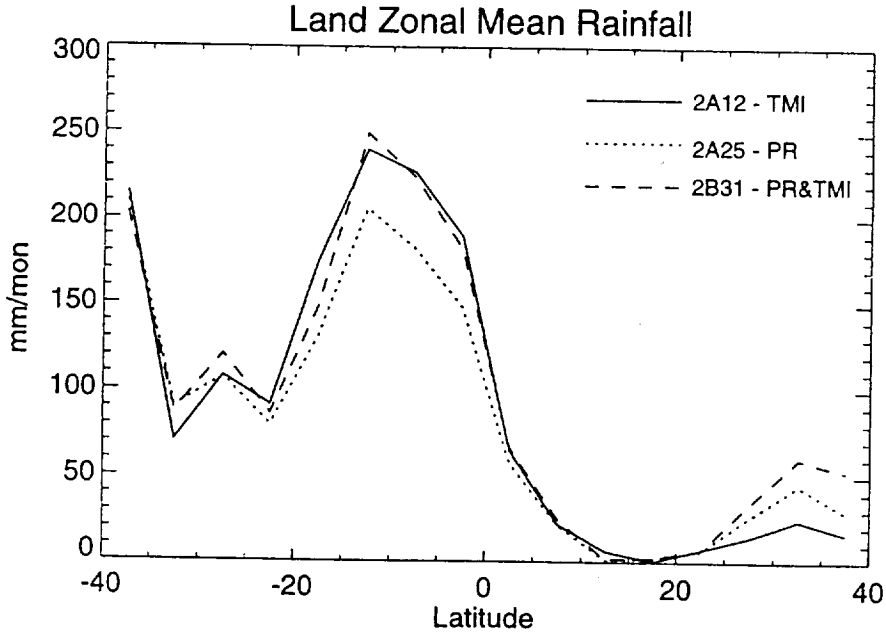

Figure 4

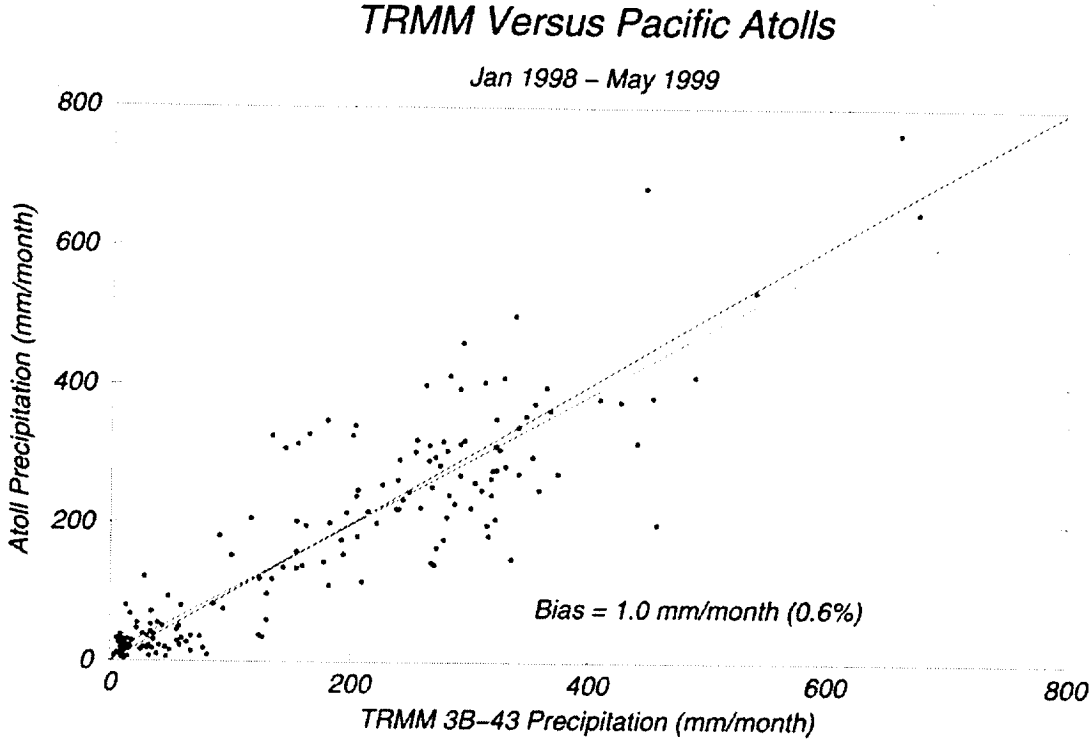

5a

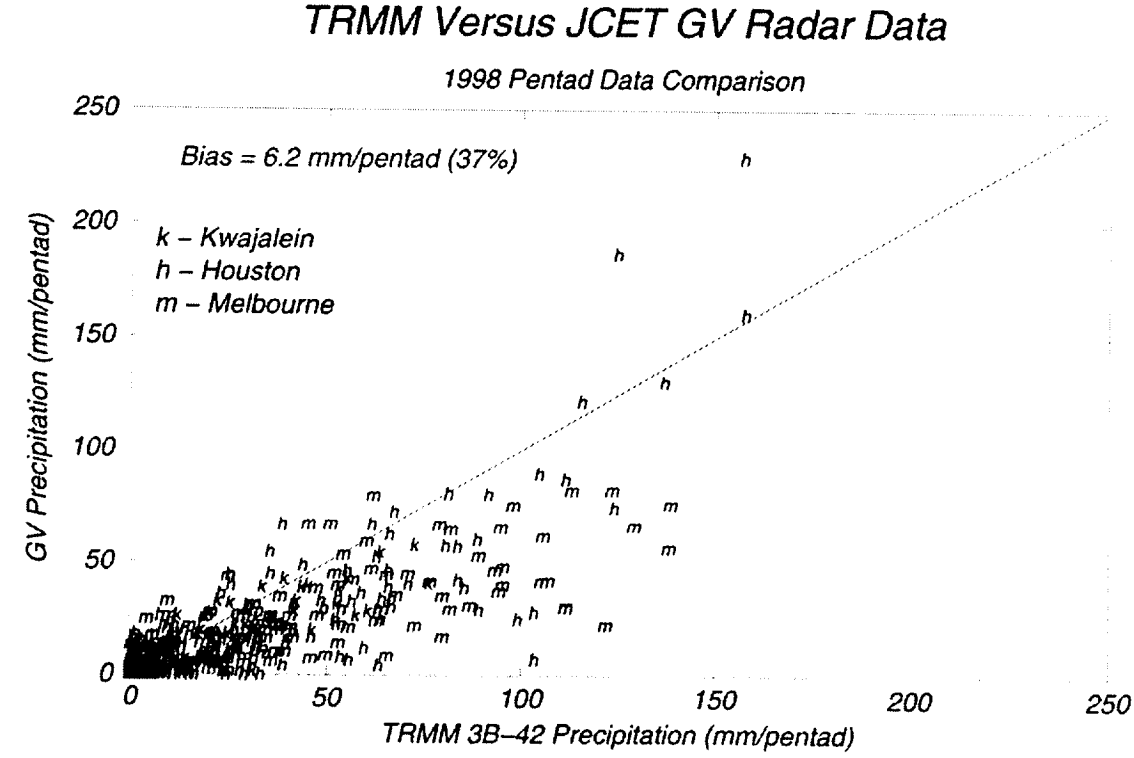

5b

Figure 5a-b

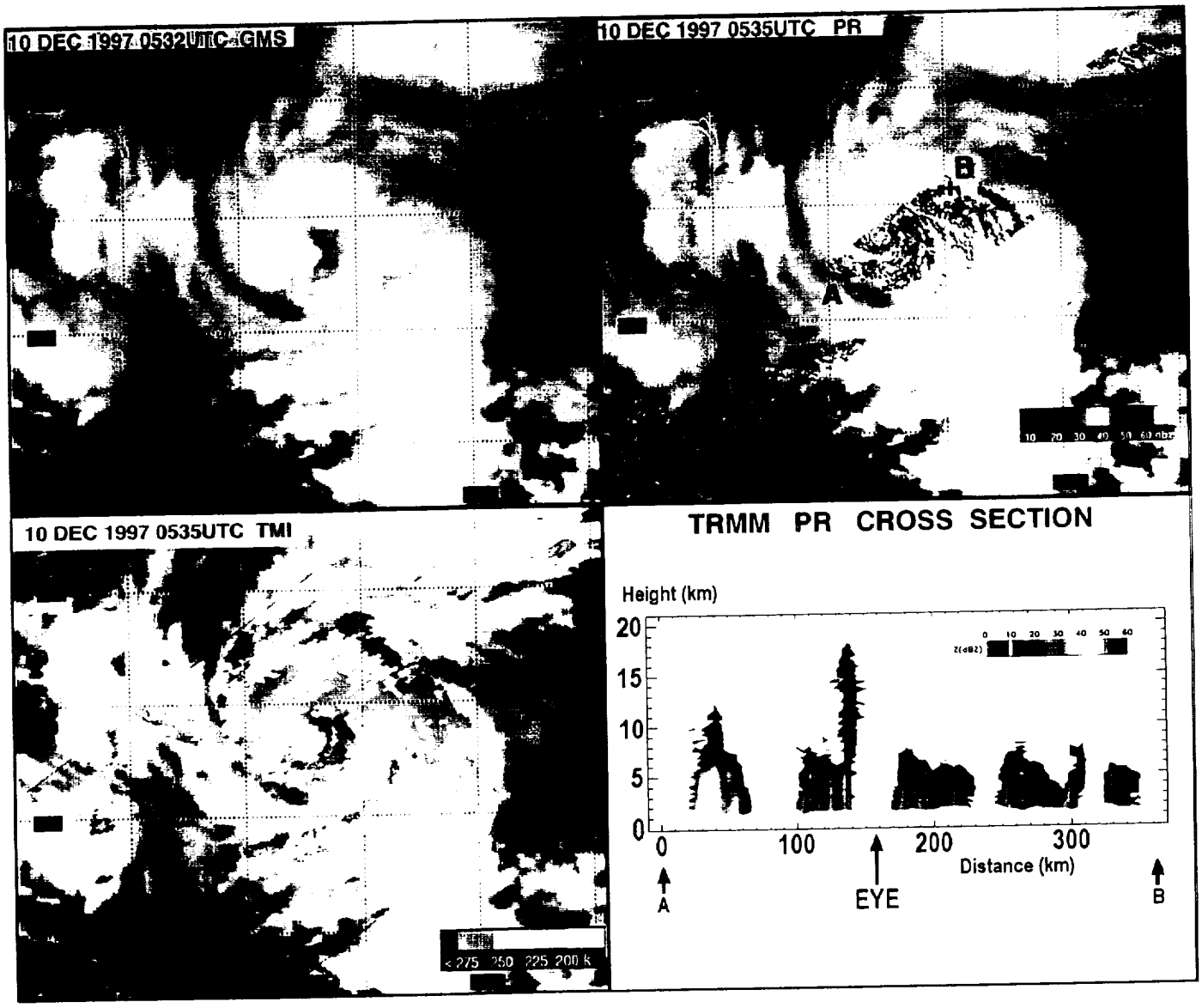
10 DEC 1997 0532UTC GMS
10 DEC 1997 0535UTC PR
B
A
10 DEC 1997 0535UTC TMI
TRMM PR CROSS SECTION
Height (km)
20
15
10
5
0
0
100
200
300
Distance (km)
A
EYE
B

Figure 6

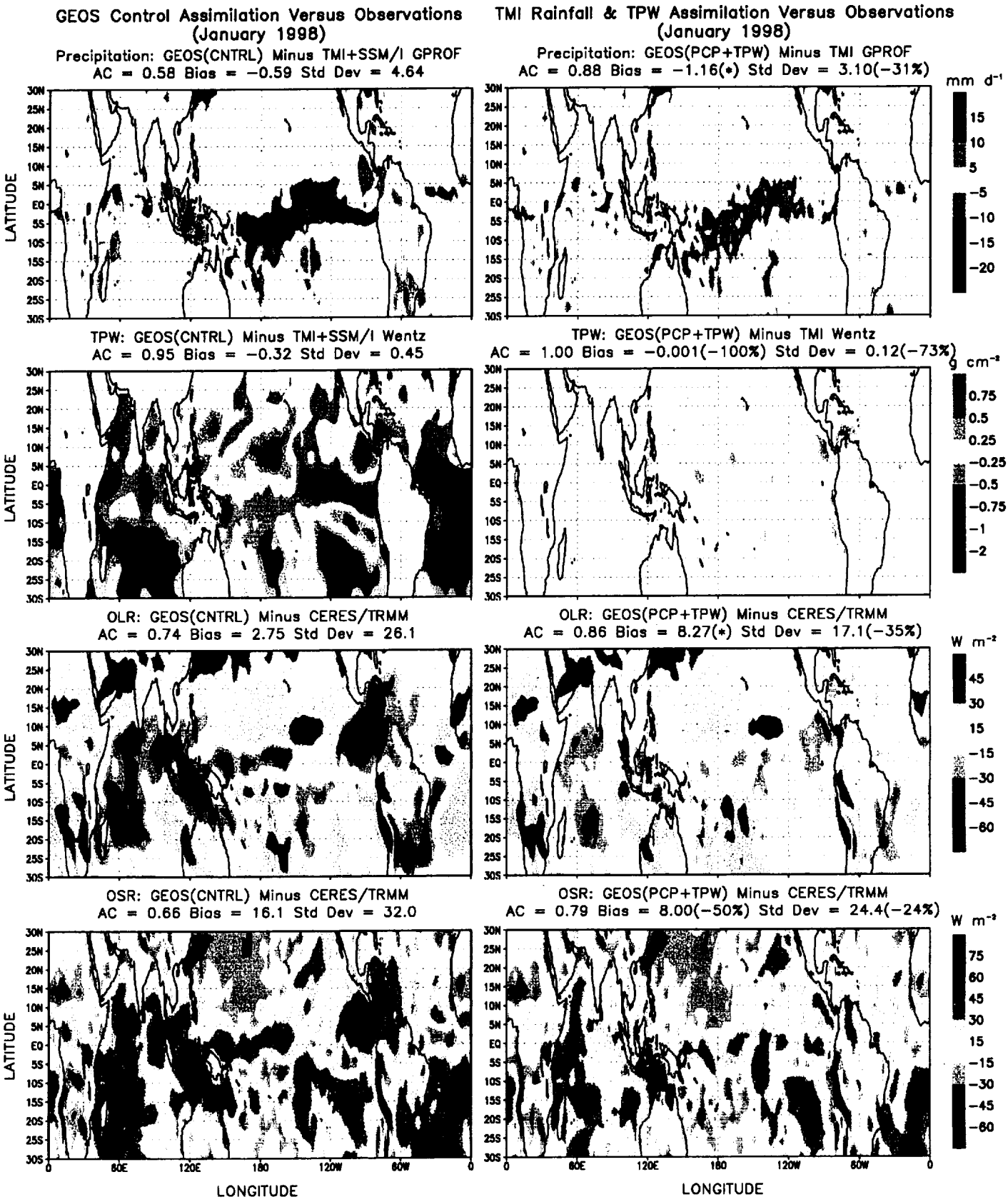
GEOS Control Assimilation Versus Observations
(January 1998)
TMI Rainfall & TPW Assimilation Versus Observations
(January 1998)
Precipitation: GEOS(CNTRL) Minus TMI+SSM/I GPROF
AC = 0.58 Bias = −0.59 Std Dev = 4.64
Precipitation: GEOS(PCP+TPW) Minus TMI GPROF
AC = 0.88 Bias = −1.16(*) Std Dev = 3.10(−31%)
mm d⁻¹
15
10
5
−5
−10
−15
−20
TPW: GEOS(CNTRL) Minus TMI+SSM/I Wentz
AC = 0.95 Bias = −0.32 Std Dev = 0.45
TPW: GEOS(PCP+TPW) Minus TMI Wentz
AC = 1.00 Bias = −0.001(−100%) Std Dev = 0.12(−73%)
g cm⁻²
0.75
0.5
0.25
−0.25
−0.5
−0.75
−1
−2
OLR: GEOS(CNTRL) Minus CERES/TRMM
AC = 0.74 Bias = 2.75 Std Dev = 26.1
OLR: GEOS(PCP+TPW) Minus CERES/TRMM
AC = 0.86 Bias = 8.27(*) Std Dev = 17.1(−35%)
W m⁻²
45
30
15
−15
−30
−45
−60
OSR: GEOS(CNTRL) Minus CERES/TRMM
AC = 0.66 Bias = 16.1 Std Dev = 32.0
OSR: GEOS(PCP+TPW) Minus CERES/TRMM
AC = 0.79 Bias = 8.00(−50%) Std Dev = 24.4(−24%)
W m⁻²
75
60
45
30
15
−15
−30
−45
−60
LATITUDE
30N
25N
20N
15N
10N
5N
EQ
5S
10S
15S
20S
25S
30S
0
60E
120E
180
120W
60W
LONGITUDE

Figure 7

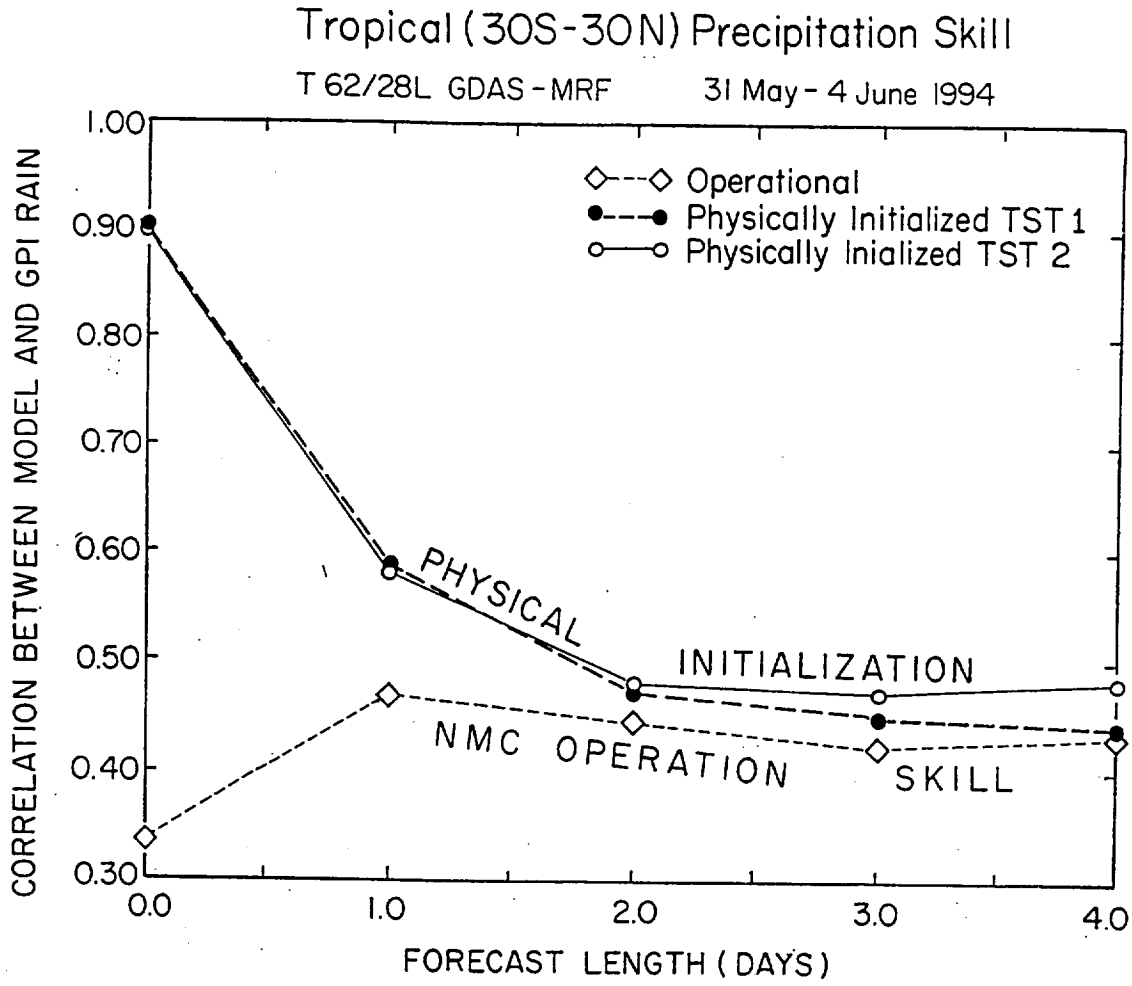
Tropical (30S-30N) Precipitation Skill
T 62/28L GDAS - MRF
31 May - 4 June 1994
Operational
Physically Initialized TST 1
Physically Inialized TST 2
PHYSICAL
INITIALIZATION
NMC OPERATION
SKILL
CORRELATION BETWEEN MODEL AND GPI RAIN
1.00
0.90
0.80
0.70
0.60
0.50
0.40
0.30
0.0
1.0
2.0
3.0
4.0
FORECAST LENGTH (DAYS)

Figure 8

Figure 9

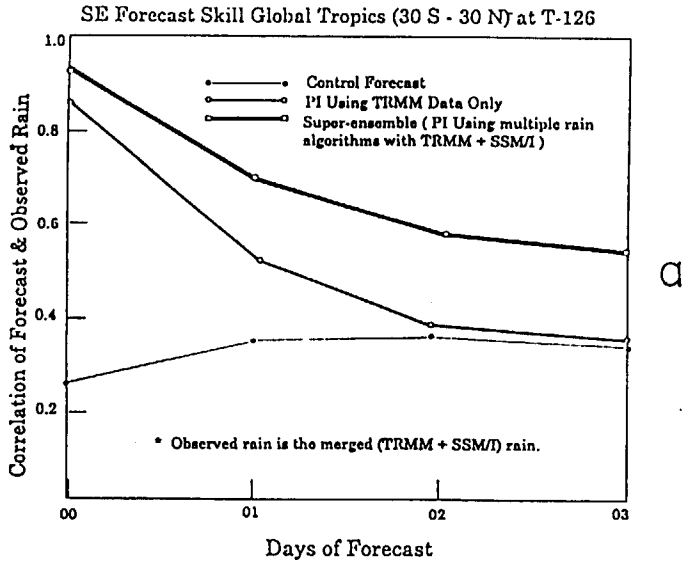

a

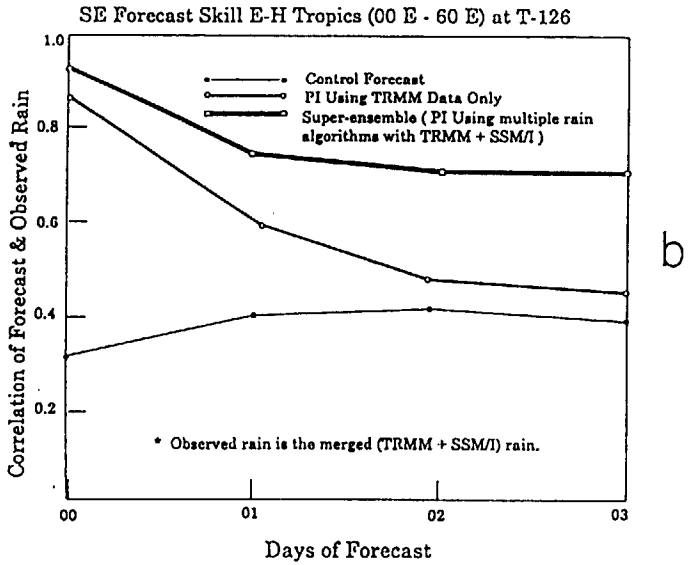

b

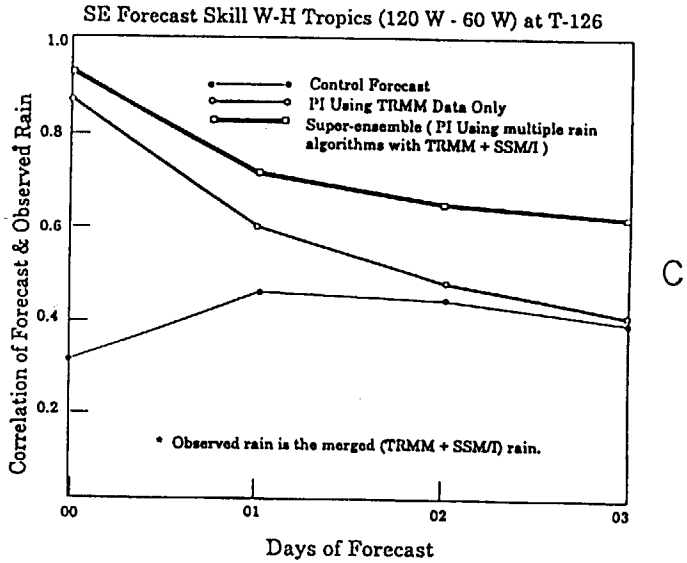

c

Fig. 4. Skill of the precipitation forecasts over
a) Global Tropics
b) Tropical Africa (0-60E)
c) Tropical Americas (120W-60W)
For control forecast, physical initialization using TRMM data only, and superensemble forecasts where the TRMM plus SSM/I rain rates are used as a benchmark. Abscissa denotes days of forecast.

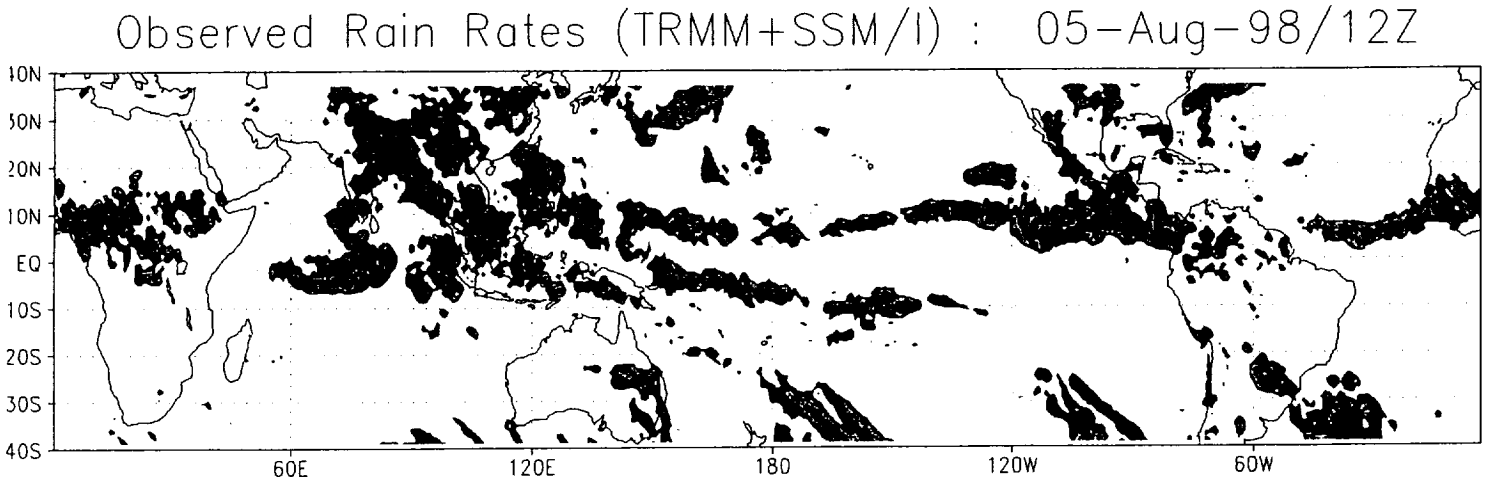
Observed Rain Rates (TRMM+SSM/I) : 05-Aug-98/12Z
40S
30S
20S
10S
EQ
10N
20N
30N
40N
60E
120E
180
120W
60W

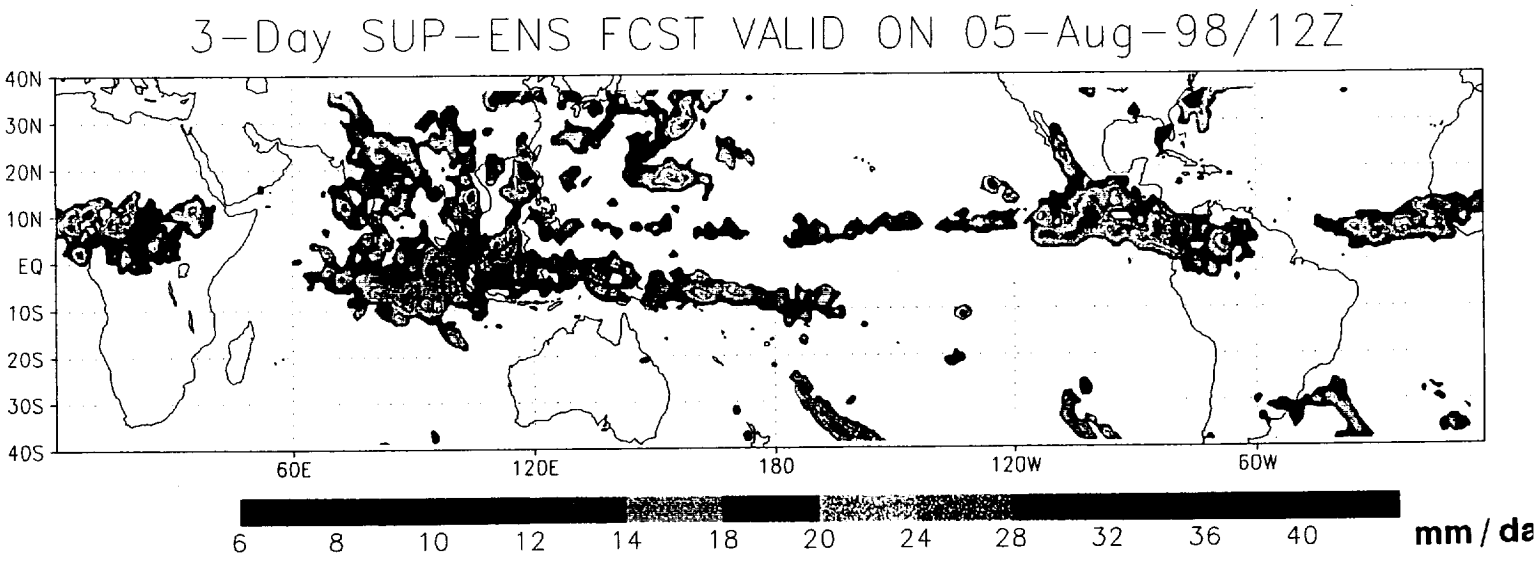
3-Day SUP-ENS FCST VALID ON 05-Aug-98/12Z
40S
30S
20S
10S
EQ
10N
20N
30N
40N
60E
120E
180
120W
60W
6
8
10
12
14
18
20
24
28
32
36
40
mm / da

Figure 10

Table 1: Goals of TRMM established by the Science Steering Group in 1986.

TABLE 1 - TRMM GOALS

I. To advance the earth science system objective of understanding the global energy and water cycles by providing distributions of rainfall and latent heating over the global tropics.

II. To understand the mechanisms through which changes in tropical rainfall influence global circulation, and to improve ability to model these processes in order to predict global circulations and rainfall variability at monthly and longer time scales

III. To provide rain and latent heating distributions to improve the initialization of models ranging from 24 hour forecasts to short-range climate variations

IV. To help understand, diagnose and predict the onset and development of the El Niño, Southern Oscillation and the propagation of the 30-60 day oscillations in the tropics

V. To help understand the effect that rainfall has on the ocean thermohaline circulations and the structure of the upper ocean

VI. To allow cross-calibration between TRMM and other sensors with life expectancies beyond that of TRMM itself

VII. To evaluate the diurnal variability of tropical rainfall globally

VIII. To evaluate a space-based system for rainfall measurement

---

Table 2: TRMM SENSOR SUMMARY - RAIN PACKAGE

MICROWAVE RADIOMETER (TMI)	RADAR (PR)	VISIBLE/INFRARED RADIOMETER (VIRS)
10.7, 19.3, 21.3, 37.0, 85.5GHz(dual polarized except for 21.3 V-only) 10x7 km FOV at 37 GHz	13.8 GHz 4.3 km footprint 250 m vertical res.	0.63, 1.61, 3.75, 10.8 and 12 μm @ 2.2 km resolution
Conically scanning (53° inc)	Cross-track scanning	Cross-track scanning
760 km swath	215 km swath	720 km swath

Additional Instruments belonging to the Earth Observing System: CERES (Cloud & Earth Radiant Energy System) & LIS (Lightning Imaging Sensor)

Table 3: Calibration parameters used for TMI brightness temperature corrections.

	ε	T_0 (K)	$\Delta T_{A,\,pred}$	$\Delta T_{A,\,obs}$
11V	0.0370	302.34	11.08	11.1
11H	0.0284	290.41	8.16	9.9
19V	0.0370	302.34	11.08	12.4
19H	0.0284	290.41	8.16	12.3
21V	0.0377	294.64	11.01	13.5
37V	0.0375	296.15	11.02	13.2
37H	0.0274	294.68	8.01	12.2
85V	0.0396	279.61	10.96	13.7
85H	0.0277	239.65	6.57	13.0

Table 4: TRMM Satellite Products

Name	Ref. no.	Purpose
Level 2 data		
Surface cross-section	2A-21	Radar surface scattering cross-section/total path attenuation.
PR Rain type	2A-23	Type of rain (conv/strat) and height of bright band.
TMI profiles	2A12	Sfc. rainfall and 3-D structure of hydrometeors and heating over TMI swath.
PR profiles	2A-25	Sfc rainfall and 3-D structure of hydrometeors over PR swath
PR/TMI Combined	2B31	Sfc. rainfall and 3-D structure of hydrometeors derived from TMI and PR simultaneously
Level 3 data		
TMI monthly rain	3A-11	Monthly 5° rainfall maps - ocean only.
PR monthly avg.	3A25	Monthly 5° rainfall and structure statistics from PR
PR Statistical	3A26	PR monthly rain accumulations - statistical method.
PR/TMI monthly avg.	3B31	Monthly accumulation of 2B31 products & ratio of this product with accumulation of 2A12 in overlap region.
TRMM & other Satellites	3B42	Geostationary precip. data calibrated by TRMM. daily, 1° resolution
TRMM & other Data	3B43	TRMM, calibrated IR and gauge products – data merged into single rain product. Monthly, 1° res.

Table 5. Description of the primary GV sites. All radars are Dopplerized. Also listed are the number of tipping bucket gauges that measure 1-min rain rates, which have been used in rain map production at GSFC.

Site	Radar characteristics	No. of gauges
Kwajalein Atoll, Republic of Marshall Islands (8.72 N, 167.73 E)	WSR-93D 10 cm polarized	9
Darwin, Australia (12.25 S, 131.04 E)	BMRC/NCAR C-POL 5 cm polarized	20
Melbourne, Florida (28.11 N, 80.65 W)	WSR-88D 10 cm	80
Houston, Texas (29.47 N, 95.08 W)	WSR-88D 10 cm	80

Table 6. Summary of TRMM field campaigns. The presence of profilers (P), radiosondes (soundings, S), rain gauges (R), disdrometers (D), tethersonde and surface flux tower (T), and lightning detectors (L) in each experiment are listed in the last column.

Field Experiment	Location	No. of radars	No. of aircraft	Other platforms
TEFLUN-A (TExas-FLorida UNderflight Experiment)	Texas	3	2	D, P, S, R, L
TEFLUN-B (TExas-FLorida UNderflight Experiment)	Florida	2	2	P, S, R, D, L
SCSMEX (South China Sea Monsoon Experiment)	South China Sea	2	0	S, R, D
TRMM-LBA (TRMM-Large Scale Biosphere-Atmosphere Experiment in Amazonia)	Rondonia, Brazil	2	2	P, S, R, D, T, L
KWAJEX (KWAJalein EXperiment)	Kwajalein, RMI	2	3	P, S, R, D, T